Coupled-channel interaction for intermediate-energy nucleon-nucleon reactions

Earle L. Lomon
Center for Theoretical Physics, Laboratory for Nuclear Science
and Department of Physics, Massachusetts Institute of Technology,
Cambridge, Massachusetts 02139
(Received 21 December 1981)

General effects of coupling a system to higher-mass channels are reviewed. The dominant effect is the addition of an attraction which increases with energy up to and, when the coupled channel is not in an S state, beyond inelastic threshold. This can produce resonances whose widths and inelasticities are largely determined by the resonance position. A model is presented for nucleon-nucleon channels coupled to $N\Delta$, NN^*, or $\Delta\Delta$ channels. It uses the Feshbach-Lomon nucleon-nucleon interaction and one-pion-exchange potentials plus phenomenological cores for the transition interactions. The width of the isobars is included. Good fits are obtained to NN channels for $E_L \lesssim 1$ GeV, including the "resonant" $^1D_2$ and $^3F_3$ partial waves. A structure may be present in the $^3P_0$ partial wave. In those partial waves where one-pion exchange predicts the largest transition potentials, the fit is improved by the long-range potential tails.

I. INTRODUCTION

Theory has been successful in predicting medium- and long-range nucleon-nucleon interactions for laboratory energy $E_L \lesssim 300$ MeV. This has been accomplished by field-theoretical and dispersion-theoretical derivations of effective potentials for the Schrödinger equation. In the range of accurate theoretical prediction, $r > \frac{1}{2}\mu^{-1}$, these potentials turn out to be only mildly energy-dependent and nonlocal (μ is the pion mass and we use $\hbar = c = 1$). The most complete of these theoretical interactions, known as the Paris potential,[1] has recently been shown[2] to provide a very good fit to the data with a phenomenological core that is very small for $r \gtrsim 1$ fm. The core only becomes dominant for $r < \frac{1}{2}\mu^{-1}$.

For $E_L > 400$ MeV the NN data contains structures[3,4] which cannot be caused by energy-independent potentials lacking barriers. Short-range energy dependence due to quark structure effects has been suggested.[5,6] In fact quark "bag-state" energies are only indirectly related to the experimental structures[7] and bag-model predictions of widths and inelasticities are at present only qualitative.[5,6]

Another mechanism for the production of strong energy dependence is the effect of the coupling to the isobar channels.[8] The Δ threshold is at $E_L = 632$ MeV, so that such effects *must* be present in the intermediate-energy region. This coupled-channel mechanism is the subject of the present paper and will be shown to explain the experimental features in a natural way.

The effect of the inelastic threshold is spread by the width of the isobar. This is of critical importance in fitting the data, especially that of the $^1D_2$ channel which would otherwise be elastic at the resonance.

In Sec. II we review the essential features of coupled-channel scattering and demonstrate that it provides an attraction in the lower-mass channel which increases with energy. The increase continues up to the inelastic threshold in each partial wave. When the orbital angular momentum in the higher-mass coupled channel, L', does not vanish, the effective inelastic threshold is raised. In these cases the attraction continues to increase beyond the true inelastic threshold. It is shown that the increasing attraction can cause resonances whose width and inelasticity are largely determined once the position of the resonance is fixed by the overall coupling strength. Thus the mechanism does not produce arbitrary widths and inelasticities, a certain range of these parameters being natural to the model. The qualitative effect of the isobar decay width is also discussed in Sec. II.

In order to compare meaningfully with the data a model is required which is sufficiently realistic theoretically and phenomenologically. It should correctly describe the direct nucleon-nucleon channel and quantitatively predict the data for $E_L \lesssim 300$ MeV when the coupling is ignored. For this purpose the Feshbach-Lomon interaction[9] (which is derived from one-boson and two-pion exchange with a boundary-condition core) is used in the nucleon-nucleon channel. It is extended, in Sec. III, to include transition potentials and isobar-channel potentials beyond the core and to provide boundary-condition coupling at the core. The one-pion-exchange transition potentials are described. The Feshbach-Lomon interaction has the advantage for this application that the theoretical potential does not include intermediate-isobar-state contributions. This avoids double counting when the intermediate isobar states are brought in through the coupled-channel mechanism. The coupled-channel Schrödinger equations are described in Sec. III, and the extension to nonzero-width isobars is given for those cases, most explicitly for cases in which the long-range transition potential can be ignored.

The computer program used is described in Sec. IV. Section V presents the results for all partial waves $L \leq 3$. Using coupling to the $N\Delta$ channel the experimental properties of the $^1D_2$ and $^3F_3$ resonances are reproduced. The possibly strong experimental inelasticity in the $^3P_0$ state requires both $N\Delta$ and $NN^*(1440)$ or $\Delta\Delta$ coupling. This coupling predicts a shoulder in the $^3P_0$ phase shift for $E_L \approx 550$ MeV. For the $^1S_0$ NN state the alternatives of $N\Delta$ coupling in a D wave, or $\Delta\Delta$ and NN^* coupling in an S wave, are distinguished by the currently uncertain degree of inelasticity of this state. The $^3S_1$-$^3D_1$ and $^1P_1$, $I=0$ states are shown to be well reproduced only when long-range transition interactions are employed, consistent with their large predicted one-pion-exchange transition potentials to the NN^* and $\Delta\Delta$ channels. Only the $\delta(^3F_2)$ is not well represented at medium energies by this coupled-channel extension of the Feshbach-Lomon interaction.

In the conclusion, Sec. VI, some remarks are made about the possible relation of quark bag states to these results.

II. GENERAL EFFECT OF CHANNEL COUPLING[8]

Elastic NN scattering proceeding through an $N_1^*N_2^*$ intermediate state, as in Fig. 1, is described by a term in the partial-wave dispersion relations

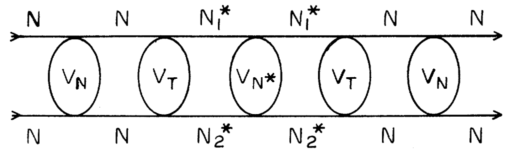

FIG. 1. Nucleon-nucleon scattering proceeding through a one- or two-isobar state $N_1^*N_2^*$ (one of which may be the nucleon). The figure represents a single passage through the isobar state but with the full diagonal NN interaction V_N, the full diagonal $N_1^*N_2^*$ interaction V_{N^*}, and the full transition interaction V_T.

$$\Delta\,\mathrm{Re}A_{\alpha L}(s)=\int_{s_i}^{\infty}\frac{\rho_{\alpha L,\alpha' L'}(s')}{s'-s}\,ds' , \tag{1}$$

where α represents all quantum numbers other than the orbital angular momentum L, the inelastic threshold is $s_i=(M_{N_1^*}+M_{N_2^*})^2$ and, by unitarity,

$$\rho_{\alpha L,\alpha' L'}(s')= |\langle \alpha' L',s' | \alpha,L,s'\rangle|^2 \times(\text{phase space}) \tag{2}$$

which is positive definite. For $s<s_i$ the denominator of the integrand is also positive definite, and the integrand is an increasing function of s for all s'. Hence the effect of coupling, as given by the discontinuity on the inelastic cut, is to add attraction to the NN channel, the amount of attraction increasing with energy up to the inelastic threshold. For normally strong interactions the numerator is sufficiently large so that resonances may often result. When $s>s_i$ the denominator has contributions of both signs and the attractive effect weakens. However near inelastic threshold the angular momentum barrier keeps ρ small when

$$(s-s_i)^{1/2}<(2L'+1)M_{\mathrm{ex}}^T , \tag{3}$$

where M_{ex}^T is the effective exchanged mass in the transition interaction. This extends the increasing interaction beyond s_i and may produce partially inelastic resonances above s_i, except for $L'=0$. When $L'=0$ the numerator varies more slowly than the denominator for $s \approx s_i$, and the attractive contribution decreases for $s>s_i$ (see Appendix A).

As noted in Ref. 8 the change $\Delta A_{\alpha L}(s'')$ on the elastic and unphysical cuts induced by the discontinuity of the inelastic cut, as given in Eq. (1), will in turn induce a change in the amplitude at s. This second-order effect may cancel some of the attraction, but cannot reverse it.

In the approximation that the integral in Eq. (1) is dominated by the first peak in the integrand as given in Eq. (3), then

$$\Delta A_{\alpha L}(s) \sim [s_i + (2L'+1)^2 (M_{\rm ex}^T)^2 - s]^{-1} \rho_{\max} \qquad (4)$$

so that the larger the range of V_T (i.e., the smaller $M_{\rm ex}^T$) the stronger the energy dependence. It follows that the width of a produced resonance depends on the range and strength of the transition interaction and on the orbital angular momentum in the inelastic channel. The effects of the diagonal interactions in each channel on the energy dependence are only indirect, hence the resonance width is insensitive to the parameters of the diagonal interaction. In fact the strength of the diagonal interaction in each channel most affects the energy dependence near its threshold. Hence resonance widths and inelasticities can only be affected moderately unless the resonance overlaps with the relevant threshold. The threshold energy dependences are usually independent information. But when a resonance overlaps inelastic threshold the asymmetry as well as the width of the resonance will be affected. Therefore, once the constraints of threshold behavior and resonance position are taken into account, the resonance width and inelasticity are predictions of the qualitative nature of the model and of physically bounded parameters such as the force range and the coupled orbital angular momentum.

The estimate of the integral given by Eq. (4) also indicates that the inelastic physical cut contribution is likely to be more important to the energy dependence than the unphysical (exchange) cut contribution well down into the region between elastic and inelastic thresholds.[8]

In the next section the effect of the width of the isobars will be taken into account by coupling to a continuum of channels with different isobar masses, weighting the coupling according to their Breit-Wigner distribution. This will affect the predictions in two obvious ways: (i) The position of an induced resonance will be a convolution of the width due to a "point" isobar and the width of the isobar. (ii) The inelasticity will extend below the threshold for production of the "point" isobar down to the threshold for pion production. The modifications are most important when a resonance is predicted near the "point" isobar production threshold, or when the resonance would be very narrow if the isobar width was neglected.

Green *et al.*[10] take the width into account by using a complex isobar mass in the coupled Schrödinger equations. In the present method the equations remain real, and the ambiguities in the choice of $\Gamma(E)$ which appear in Ref. 10 do not occur here.

Equation (1) describes two other mechanisms, besides the general coupled-channel effect discussed above, for introducing structure into the NN amplitude. The nature of the branch point at s_i is determined by $\rho \sim (s'-s_i)^{L'}$, giving rise to a cusp in the cross section which has a discontinuous $(L'+1)$-order derivative. The cusp is difficult to observe for $L'>0$, but may be substantial for $L'=0$ when Γ is small. The remaining mechanism comes into play only if the diagonal coupling in the higher-mass channel is strongly enough attractive to bind the $N_1^* N_2^*$ system. In the presence of coupling the bound state leaks into the NN channel causing it to resonate. This gives rise to large effects but may be expected to be rare as particle bound states are rare. It was invoked as the cause of the Y_0^* resonance by Dalitz and Tuan,[11] but is not necessary to the explanation.[12] These special coupled-channel resonances have very different characteristics from the general type described above in that their resonance position is fixed by the strength of the diagonal $N_1^* N_2^*$ interaction, while the width is independently determined by the transition interaction.[8,13]

The predictions of similar channel-coupling models have been compared with several resonance effects in the pion-pion,[14] pion-nucleon,[15–17] kaon-nucleon,[18] and antikaon-nucleon[12] reactions with some success. Although alternative mechanisms exist to explain many of these resonances, the channel coupling results seem particularly appropriate for the "exotic" resonances. Nonresonant NN effects have also been examined.[19] Recently other channel-coupling models have been used to examine the nucleon-nucleon structures.[20,21]

III. A COUPLED-CHANNEL MODEL FOR THE NUCLEON-NUCLEON REACTION

A. Description of model

The effect on the NN channel of the coupling to isobars depends mainly, as discussed above, on the strength and range of the transition potential and on the threshold energy and orbital angular momentum of the inelastic channel. A model incorporating the nearby thresholds and the dominating (i.e., the smallest) L' with a reasonable interaction range will, when the transition interaction strength is adjusted to a resonance position or other relevant feature, give semi-quantitatively correct results for the structure. However the NN diagonal interaction must be realistic (both theoretically and phenomenologically) as a baseline against which to see the effect of turning on the interchannel coupling and to obtain the correct detailed behavior for the first few hundred MeV above elastic threshold. For this purpose we choose the Feshbach-Lomon interaction[9] for which the medium- and long-range potential is constructed from one-boson and two-pion exchanges and which fits the nucleon-nucleon data well up to $E_L \approx 300$ MeV.

The potential includes the single exchange of pions, η, ρ, and ω mesons with coupling constants determined by independent meson-nucleon experiments and/or by particle theory. The two-pion-exchange contribution was obtained by the semirelativistic method of Breuckner and Watson[22] and of Taketani, Machida, and Ohnuma.[23] It includes only nucleons, antinucleons, and pions in intermediate states. The semirelativistic approximation for the intermediate states is a deficiency; however, the resulting potential is similar to those derived in a completely relativistic manner, such as the Paris[1] and Partovi-Lomon[24] potentials. The absence of contributions from intermediate isobar states is an important advantage when isobar channels are explicitly coupled because it avoids double counting. In the Paris potential the contributions of nucleon and isobar intermediate states are inextricably mixed in the pion-nucleon amplitudes. The Partovi-Lomon potential is theoretically suitable but is complicated in form and has not been fitted with a phenomenological core to the low-energy data.

In Ref. 24 it is demonstrated that there is a systematic expansion of the potential, arising from the Blankenbecler-Sugar reduction, in which the noniterative corrections to the coupled-channel interaction are put into the diagonal potentials. This is in contrast to other prescriptions[10,25] in which the transition potential is modified from its simple relativistic form. In this paper corrections to the simple forms will also be omitted from the diagonal potentials, as important contributions (from two-pion exchange, etc.) are in any case not available now for any but the NN diagonal component. We hope to consider the effects of fully theoretical transition and isobar potentials in a later article. The object of the present paper is the exploration of the importance of channel coupling in the nucleon-nucleon interaction, and the formulation of a physically plausible but partly phenomenological interaction which will fit the data in the intermediate- and low-energy regions simultaneously. For this purpose we have kept the NN diagonal interaction realistic and have treated transition and isobar channel interactions more phenomenologically, but of physical range. Where the one-pion long-range tail of the transition potential is included we have used the theoretical form and strength, parametrizing only the shorter-range interaction.

B. Model formalism

The explicit form of the Feshbach-Lomon potential is in Ref. 9, pp. 107–108. The Feshbach-Lomon core is in the form of an energy-independent boundary condition, rather than a potential. For the uncoupled partial waves with $L=J$ one has the Schrödinger equation and boundary condition

$$-\frac{d^2U_J}{dr^2}+\frac{J(J+1)}{r^2}U_J+MV_{J,J}(r)U_J=k^2U_J \;, \tag{5}$$

$$r_0\left[\frac{dU_J}{dr}\right]_{r_0}=f_JU_J(r_0) \;, \tag{6}$$

while for the tensor coupled channels with $L=J\pm1$

$$-\frac{d^2U_{J-1}}{dr^2}+\frac{J(J-1)}{r^2}U_{J-1}+MV_{J-1,J-1}(r)U_{J-1}+MV_{J-1,J+1}(r)U_{J+1}=k^2U_{J-1} \;, \tag{7a}$$

$$-\frac{d^2U_{J+1}}{dr^2}+\frac{(J+1)(J+2)}{r^2}U_{J+1}+MV_{J-1,J+1}(r)U_{J-1}+MV_{J+1,J+1}(r)U_{J+1}=k^2U_{J+1} \;, \tag{7b}$$

$$r_0\frac{dU_{J-1}}{dr_0}=f_{J-1,J-1}U_{J-1}(r_0)+f_{J-1,J+1}U_{J+1}(r_0) \;, \tag{8a}$$

$$r_0\frac{dU_{J+1}}{dr_0}=f_{J-1,J+1}U_{J-1}(r_0)+f_{J+1,J+1}U_{J+1}(r_0) \;. \tag{8b}$$

The $U_L(r)$ behave asymptotically as linear combinations of the $rh_L^{(i)}(kr)$, $i=1,2$ or of the Coulomb functions $F_L(K,r)\pm iG_L(K,r)$. k^2 is the relativistic momentum of each nucleon in the center of mass. M is twice the reduced mass of the nucleons. The $V_{L,L'}$ are determined by the central, spin-spin, spin-orbit, and tensor potentials in the usual way, including Coulomb forces in the diagonal terms.

The extension to include isobar channels is a straightforward generalization of the tensor coupled case, allowing for the dependence of the momentum on the masses in the channels:

$$-\frac{d^2U_i}{dr^2}+\frac{L_i(L_i+1)}{r^2}U_i+\sum_j M_i V_{ij}(r)U_j = {k_i}^2 U_i \ , \tag{9}$$

$$r_0\frac{dU_i}{dr_0}=\sum_j f_{ij}U_j(r_0) \tag{10}$$

with

$$\sqrt{s}\equiv W=({M_{ia}}^2+{k_i}^2)^{1/2}+({M_{ib}}^2+{k_i}^2)^{1/2} \ , \tag{11}$$

where the real quantities $V_{ij}=V_{ji}$, $f_{ij}=f_{ji}$, M_{ia} and M_{ib} are the masses of the two particles in channel i and M_i is twice their reduced mass, and W is the barycentric energy. As it is usual to quote experimental NN results in laboratory energy we note that relativistically,

$$k^2=E_L M^2(2M_B)^{-1}\left[1+\frac{E_L}{2M_B}\right]\left[1+\frac{M^2E_L}{2M_BM_T}\right]^{-1} , \tag{12}$$

where M_B is the beam-nucleon mass and M_T is the target-nucleon mass. For $M_B=M_T$, Eq. (12) becomes $k^2=(M/2)E_L$, exactly as in the nonrelativistic case.

As the $N^*(1440)$ has nucleonic properties ($s=\frac{1}{2},T=\frac{1}{2}$) the one-pion-exchange (OPE) transition potential for $NN\leftrightarrow NN^*(1440)$ is like the OPE nucleon-nucleon potential except for the coupling constant:

$$V^{\rm OPE}_{NN,NN^*}(r)=\frac{f_N f_*}{4\pi}\frac{\mu}{3}\vec{\tau}_N\cdot\vec{\tau}_* \times[\vec{\sigma}_N\cdot\vec{\sigma}_* V_0(x)+S^{\rm I}_{12}V_2(x)] \ , \tag{13}$$

where $f_N\equiv g_{NN\pi}(\mu/2M)$ is the pseudovector $\pi N\bar{N}$ coupling constant [we use $(g_{NN\pi})^2/4\pi=14.94$], f_* is the pseudovector $\bar{N}N^*\pi$ coupling constant, $x=\mu r$,

$$S^{\rm I}_{12}=3(\vec{\sigma}_*\cdot\hat{r})(\vec{\sigma}_N\cdot\hat{r})-\vec{\sigma}_*\cdot\vec{\sigma}_N \ ,$$

$$V_0(x)=x^{-1}e^{-x} \ ,$$

and

$$V_2(x)=(x^{-1}+3x^{-2}+3x^{-3})e^{-x} \ .$$

The OPE transition potentials for $NN\leftrightarrow N\Delta$ and for $NN\leftrightarrow\Delta\Delta$ are as given by Sugawara and von Hippel,[26] ignoring energy-dependent factors which approach unity as $M_\Delta\to M$.

$$V^{\rm OPE}_{NN,N\Delta}=\frac{f_N f_\Delta}{4\pi}\frac{\mu}{3}\vec{\tau}_N\cdot\vec{\rm T}[\vec{\sigma}_N\cdot\vec{\rm S}V_0(x)+S^{\rm II}_{12}V_2(x)] \ , \tag{14}$$

$$V^{\rm OPE}_{NN,\Delta\Delta}=\frac{(f_\Delta)^2}{4\pi}\frac{\mu}{3}\vec{\rm T}_1\cdot\vec{\rm T}_2[\vec{\rm S}_1\cdot\vec{\rm S}_2V_0(x)+S^{\rm III}_{12}V_2(x)] \ , \tag{15}$$

where $\vec{\rm T}$ and $\vec{\rm S}$ are the transition isotopic spin and spin operators defined in Ref. 26, f_Δ is the $\bar{N}\Delta\pi$ coupling constant, and

$$S^{\rm II}_{12}=3(\vec{\sigma}_N\cdot\hat{r})(\vec{\rm S}\cdot\hat{r})-\vec{\sigma}_N\cdot\vec{\rm S} \ ,$$

$$S^{\rm III}_{12}=3(\vec{\rm S}_1\cdot\hat{r})(\vec{\rm S}_2\cdot\hat{r})-\vec{\rm S}_1\cdot\vec{\rm S}_2 \ .$$

Explicit expressions for the operators appearing in Eqs. (14) and (15) are given in Ref. 26 in terms of 3-J, 6-J, and 9-J symbols.

We use f_* and f_Δ as given by the elastic πN scattering widths

$$\frac{{f_\Delta}^2}{4\pi}=48\mu^2{M_\Delta}^{-3}\Gamma^{\rm el}_\Delta\left[\left[1+\frac{M}{M_\Delta}\right]^2-\left[\frac{\mu}{M_\Delta}\right]^2\right]^{-1}\left[1-\left[\frac{M+\mu}{M_\Delta}\right]^2\right]^{-3/2}\left[1-\left[\frac{M-\mu}{M_\Delta}\right]^2\right]^{-3/2} , \tag{16}$$

$$\frac{{f_*}^2}{4\pi}=\tfrac{16}{3}\mu^2{M_*}^{-3}\Gamma^{\rm el}_*\left[\left[1+\frac{M}{M_*}\right]^2-\left[\frac{\mu}{M_*}\right]^2\right]^{-1}\left[1-\left[\frac{M+\mu}{M_*}\right]^2\right]^{-3/2}\left[1-\left[\frac{M-\mu}{M_*}\right]^2\right]^{-3/2} . \tag{17}$$

With $M_\Delta=1232$ MeV, $\Gamma_\Delta^{el}=\Gamma_\Delta=115$ MeV, one obtains ${f_\Delta}^2/4\pi=0.35$ and $f_N f_\Delta/4\pi=0.165$. Using the most recent values for the $P_{(1/2)(1/2)}$ resonance,[27] $M_*=1440$ MeV, $\Gamma_*^{el}=0.68\Gamma_*=0.68\times 340$ MeV, one obtains ${f_*}^2/4\pi=0.015$ and $f_N f_*/4\pi=0.034$.

Because of its theoretical origin the Feshbach-Lomon potential is not altered in this application. However, the constant elements of the f matrix are phenomenological and the old values of Ref. 9 are changed to compensate for the residual effect at elastic threshold of coupling to isobar channels.

C. Special case: Vanishing transition-potential tail

To obtain a simple realization of the f-matrix-renormalization effect, as well as the important energy-dependent properties of coupled channels inherent in Eq. (1), we temporarily ignore the long-range, transition-potential interaction. This has no qualitative effect on the results and, as we will see, is often unimportant quantitatively.

If the incoming channel is $i=1$, then, for $i>1$,

$$\lim_{r\to\infty} U_i(r)=\begin{cases} Arh_{L_i}^{(1)}(Kr) \ \text{ or} \\ A\,[F_{L_i}(k,r)+iG_{L_i}(k,r)]\ . \end{cases}$$

Because of the absence of transition potentials one may obtain $U_i(r_0)=A_iJ_{L_i}^+(r_0)$, the outgoing $J_{L_i}^+$ function satisfying the above limit with $A=1$ and the equation

$$-\frac{d^2J_{L_i}^+}{dr^2}+\frac{L_i(L_i+1)}{r^2}J_{L_i}^+ + V_{ii}(r)J_{L_i}^+ = {k_i}^2 J_{L_i}^+ \ . \tag{18}$$

Inserting these results into Eq. (10), $i=2,3,\ldots N$, one can solve for the $N-1$ unknown $A_i, i=2,\ldots N$ and obtain

$$r_0\frac{dU_1}{dr_0}=f^{\text{eff}}U_1(r_0)\ , \tag{19}$$

where f^{eff} is explicitly given by the $J_{L_i}^+$ and the $dJ_{L_i}^+/dr$ for $i=2,\ldots N$ and all the f_{ij}. Equation (19) together with Eq. (9) for $i=1$ determines U_1 and the S matrix in the same way as for a single-channel problem, except that f^{eff} is energy dependent and complex. When $N=2$ it is easily seen that

$$f^{\text{eff}}(k_1)=f_{11}-\frac{{f_{12}}^2}{f_{22}+\theta_2^+[k_2(k_1)]}\ , \tag{20}$$

where

$$\theta_2^+=-\frac{r_0}{J_{L_2}^+(k_2,r_0)}\frac{dJ_{L_2}^+(k_2,r)}{dr_0}\ . \tag{21}$$

The general properties of J_L^+ functions are such that θ_2^+ is real when k_2 is imaginary, i.e., below inelastic threshold.[8] This guarantees one-channel unitarity in the elastic region. If the fit at k_0 near elastic threshold with $f_{12}=0$ required $f_{11}=f_0$, we can restore that fit with $f_{12}\neq 0$, by adjusting f_{11} so that

$$f_{11}=f_0+\frac{{f_{12}}^2}{f_{22}+\theta_2^+[k_2(k_0)]}\ . \tag{22}$$

It can also be shown[8] that above inelastic threshold $\text{Im}\, f^{\text{eff}}\leq 0$ satisfying multichannel unitarity and ensuring that only bound state S-matrix poles are on the physical sheet. When $V_{22}=0$ then the J_L^+ functions reduce to Hankel functions and it can be shown that

$$\theta_2^+(0)=L_2 \ \text{and}\ \frac{d}{d\chi}[\theta_2^+(i\chi)]>0 \quad \text{for}\ \chi>0\ . \tag{23}$$

The properties of Eqs. (20) and (23) require[8] that $df^{\text{eff}}/dk_1<0$, and if $f_{22}>-L_2$, $f^{\text{eff}}(k_1)<f_{11}$ when k_1 is in the elastic region. As a smaller f^{eff} implies more attraction we here see the attractive effect of coupled channels, becoming more attractive with increasing energy, in an explicit way. If $f_{22}<-L_2$ that result is not changed, but a pole is introuced into f^{eff} in the elastic region, which induces a Dalitz-Tuan-type[11] quasi-bound-state resonance.[8] If $V_{22}\neq 0$ the critical value of f_{22} will shift from $-L_2$ according to the strength and sign of the potential. Also the range dependence of the potential will modify the rate of increase of attraction with energy.

For $N>2$, f^{eff} has simple forms for several interesting cases.[8] If $f_{ij}=0$ unless $i=j$ or $i=1$, then

$$f^{\text{eff}}(k_1)=f_{11}-\sum_{j=2}^{N}(f_{1j})^2\{f_{jj}+\theta_j^+[k_j(k_i)]\}^{-1}\ . \tag{24}$$

If $f_{ij}=0$ unless $j=i\pm 1$ or i, then

$$f^{\text{eff}}(k_1)=f_{11}-(f_{12})^2\{f_{22}^{\text{eff}}+\theta_2^+[k_2(k_1)]\}^{-1} \tag{25}$$

with

$$f_{ii}^{\text{eff}}=f_{ii}-\frac{{f_{i,i+1}}^2}{f_{i+1,i+1}^{\text{eff}}+\theta_{i+1}^+[k_{i+1}(k_1)]} \tag{26}$$

leading to a continued-fraction form, breaking off at $f_{NN}^{\text{eff}}=f_{NN}$.

D. Inclusion of isobar widths

The width of the isobar implies that the incoming NN channel is coupled to a continuum of isobar channels, each of different isobar mass. In a representation in which the isobar channels are not coupled to each other the production distribution of isobars will be proportional to the square of the strength of the NN-NN^* coupling. Therefore the square of the coupling must be proportional to the Breit-Wigner distributions of the isobar resonance, as a function of the isobar mass. Equation (9) then becomes

$$-\frac{1}{M_1}\frac{d^2U_1}{dr^2}+\frac{L_i(L_i+1)}{M_1r^2}U_1+V_{11}(r)U_1+V_{12}(r)\int_{M+\mu}^{\infty}[\mathcal{N}\rho(M_*)]^{1/2}U_2(M_*,r)dM_*=k_1{}^2U_1 \tag{27a}$$

and, for $M+\mu\le M_*<\infty$,

$$-\frac{1}{M_*}\frac{d^2U_2(M_*,r)}{dr^2}+\frac{L_2(L_2+1)}{M_*r^2}U_2(M_*,r)+V_{22}(r)U_2(M_*,r)+V_{12}(r)[\mathcal{N}\rho(M_*)]^{1/2}U_1(r)=[k_2(M_*)]^2U_2(M_*,r)\,, \tag{27b}$$

where M_* is the isobar mass, $K_2(M_*)$ is obtained from Eq. (11) by replacing M_{2a} with M, and M_{2b} with M_*:

$$\rho(M_*)=q^{2L_*+1}M_*{}^{-2L_*}\left[(\overline{M}_*{}^2-M_*{}^2)^2+\Gamma_*{}^2\frac{\overline{M}_*{}^4}{M_*{}^2}\left[\frac{q}{\bar{q}}\right]^{4L_*+2}\right]^{-1} \tag{28}$$

and

$$\mathcal{N}^{-1}=\int_{M+\mu}^{\infty}\rho(M_*)dM_*\,.$$

Here Γ_* is the isobar width, L_* is the orbital angular momentum of the pion-nucleon decay product of the isobar and q is the momentum of either decay particle in the isobar rest system. The central value of the isobar mass is $\overline{M}_*$ and $\bar{q}$ is the decay particle momentum corresponding to that mass.

Equations (27) can be solved numerically by giving M_* discrete values and treating the system as an N-channel system, with N sufficiently large.

The computer program described in the next section is limited to $N=6$ and furthermore does not take advantage in integrating the coupled equations of the simplification inherent in Eqs. (27) that $V_{ij}=0$ unless $i=j$ or $i=1$. To simplify the calculation and reduce the computing time we now treat coupling to the isobar channel continuum only through the boundary conditions, neglecting transition potential tails when the isobar width is included.[15–18] Then the same considerations that lead to Eq. (27) lead to Eq. (19) but with Eq. (20) extended to

$$f^{\text{eff}}(k_1)=f_{11}-\sum_j(f_{1j})^2\mathcal{N}_j\int_{M+\mu}^{\infty}\frac{\rho_j(M_{j*})dM_{j*}}{f_{jj}+\theta_j^+[k_j(M_{j*},k_1)]} \tag{29}$$

with the index $j=2,3,\ldots$ allowing for more than one isobar channel. The computation of θ_2^+ is required for every value of M_* used in computing the integral, which requires an order of magnitude more computing time than the zero-width case, even in this simplified version. When $W>2M+\mu$, k_2 is real for the lower part of the range of integration of M_* and f^{eff} becomes complex.

When an isobar channel is coupled to a pair of tensor coupled NN channels it is important to include the NN tensor potential. A straightforward generalization of the above procedure in which the transition potential tails to the isobar channels are ignored, leads to the two-channel problem with $V_{ij}\neq 0$, $i,j=1,2$ and

$$f_{ij}^{\text{eff}}(k_1)=f_{ij}-\sum_n f_{in}f_{jn}\mathcal{N}_n\int_{M+\mu}^{\infty}\frac{\rho_n(M_{n*})dM_{n*}}{f_{nn}+\theta_n^+[k_n(M_{n*},k_1)]}\,, \tag{30}$$

$i,j=1,2$ and $n=3,4,\ldots$.

The inclusion of the long-range transition potential tail is important when that potential is strong and we are examining the inelasticity near threshold. Fortunately the strongest long-range transition potentials are for the $I=0$ states for which the lowest isobar-channel thresholds are centered at $M_N+M_{N^*}\approx 2400$ MeV, producing little inelasticity in the energy range we consider here. Where relevant, fits are made of both types: transition tails, no width, and no transition tails, width.

IV. NUMERICAL METHODS

The basic computer program COCHASE which integrates the coupled Schrödinger equations and computes the S-matrix coefficients has been described in detail.[28] There are two main options in the published program, the general case and the special case. The general case must be used when there are off-diagonal potentials, either the NN tensor potential or transition potentials to isobar states. Equations (9) are integrated outward from r_0, finding N solution sets i of the N wave functions, corresponding to starting conditions $U_{ij}(r_0)=\delta_{ij}$ for the jth channel, $i,j=1,2,\ldots,N$. The f matrix supplies the values of

$$(d/dr_0)U_{ij}=r_0 f_{ij}U_{ij}(r_0)$$

needed to integrate the second-order equation. A Runge-Kutta integration routine then integrates the $U_{ij}(r)$ out to $r=r_f$ where r_f is chosen to be several times the interaction range (usually $r_f \gtrsim 10$ fm). At this radius a linear combination of the solutions is required to have the same logarithmic derivatives for $j>1$ as outgoing free waves $h_{L_j}^{(1)}(k_j r)$ or Coulomb waves $F_{L_j}(kr)+iG_{L_j}(k,r)$. This, together with a normalization condition on channel 1 determines the linear coefficients, which are also the production amplitudes for channels $j>1$. Comparison of the logarithmic derivative of channel 1 with $h_{L_1}^{(2)}+S_{L_1}h_{L_1}^{(1)}$ (or the Coulomb analog) at r_f then determines the S matrix for the incoming channel.

The special case takes advantage of the condition $V_{ij}=0$, $i\neq j$, to integrate one channel $j>1$ at a time to obtain the outgoing $J_{L_i}^{+}$ function [Eqs. (18)]. Beginning with outgoing Hankel or Coulomb functions at r_f it integrates each channel in to r_0. At r_0 the derivatives of $J_{L_j}^{+}$ are computed and Eqs. (10) are used to obtain the relative normalizations C_j of the $U_j(r_0)=C_j J_{L_j}^{+}(r_0)$ for $j>1$, and to obtain f^{eff} from the $i=1$ equation and Eq. (19). The channel $j=1$ is then integrated outwards to r_f. There it is matched as before to the asymptotic form and the S matrix is extracted.

The nucleon-nucleon potential is the Feshbach-Lomon potential of Ref. 9, pp. 107–108. The transition potentials and diagonal-isobar-channel potentials are coded as Yukawa forms of variable strength and range (the Ref. 28 version has been extended to include sums of Yukawa potentials of different range and Yukawa potentials times inverse powers of r in tensor forms).

To include the effect of width of the isobar the published version[28] has been extended to calculate f^{eff} by Eqs. (29) or (30). The remaining channels (with no isobar width) are then integrated outwards using the special case, or the general case if nonvanishing transition potentials exist among them. The time for the calculation is greatly increased over the no-width case because the $\theta_{L_j}^{+}$ must be found for each value of M_* in the integrands of Eqs. (29) and (30), necessitating the integration of the J_L^{+} functions each time. The expanded program is called COWP and has five options: (i) no potential coupling, nonvanishing isobar width, (ii) potential coupling between some channels and nonvanishing isobar width in others, (iii) one channel, (iv) no potential coupling, vanishing isobar widths (special case of COCHASE), and (v) potential coupling, vanishing isobar widths (general case of COCHASE).

The program is run in double precision on the IBM version of the code, and in single precision on the CDC version because of the longer word length. The phase shifts obtained are accurate to 10^{-2} degrees or better. Three-channel cases using options (i), (ii), (iv), and (v) typically take 10^2, 10^3, 1, and 10 sec, respectively, to find the S matrix on a CDC 6600 and are 5–10 times faster on a CDC 7600.

V. RESULTS FOR NN AT INTERMEDIATE ENERGY

The problem of "fitting" is complicated by the instability of the phase-shift solutions, especially for energies >515 MeV (i.e., above TRIUMF energies) where the data sets are less complete. Comparisons were made with the phase shifts obtained by Bugg *et al.*,[29] Hoshizaki,[30] Arndt,[31] and Bystricky *et al.*[32] These authors have produced several revised sets of phase shifts during the period of the present analysis. At the higher energies, in particular, there has been a need to supplement the data with information from forward dispersion relations and theoretical calculations of some imaginary phase shifts. Together with energy-dependence assumptions this makes many of the results less than convincing. However the more recent analyses have tended to agree with each other, although only qualitatively at higher energies.

Under the circumstances a least-χ^2 fit to phase shifts did not seem to be indicated. Instead the coupling parameters were varied "by hand" in order to get a fit "by eye" that seemed best in obtaining the most important and stable features of the phase-shift results.

The procedure was not arbitrary. The lowest-mass isobar channel and lowest value of L' allowed by strong selection rules were coupled to each NN partial wave. In a two-channel case, for each choice of f_{22} and f_{12}, f_{11} was chosen using Eq. (22) so that $f^{\rm eff}$ at $E_L = 0-200$ MeV was consistent with the well-known low-energy phase shifts. Then f_{12} was varied, with f_{11} in correlation, to produce the experimentally indicated phase shifts, including indicated resonances, in the intermediate energy region (200−800 MeV). Finally, a few values of f_{22} were chosen, and f_{12} and f_{11} correlated, to obtain the best overall fit, including details near the inelastic threshold. If the boundary-condition transition interaction of the strength required for the attraction needed at the higher energies (500−800 MeV) provided insufficient attraction at lower energies (200−500 MeV), that was an indication that the range of the transition interaction was too short. Then the fitting was done again with a transition-potential tail replacing all or most of f_{12}. The procedure was more complicated for a three-channel system, but similarly used the low-energy data (which consists of three quantities δ_{J-1}, δ_{J+1}, and ϵ_J) to determine three of the parameters whenever another parameter was varied.

In most cases the fit is clearly adequate quanti-

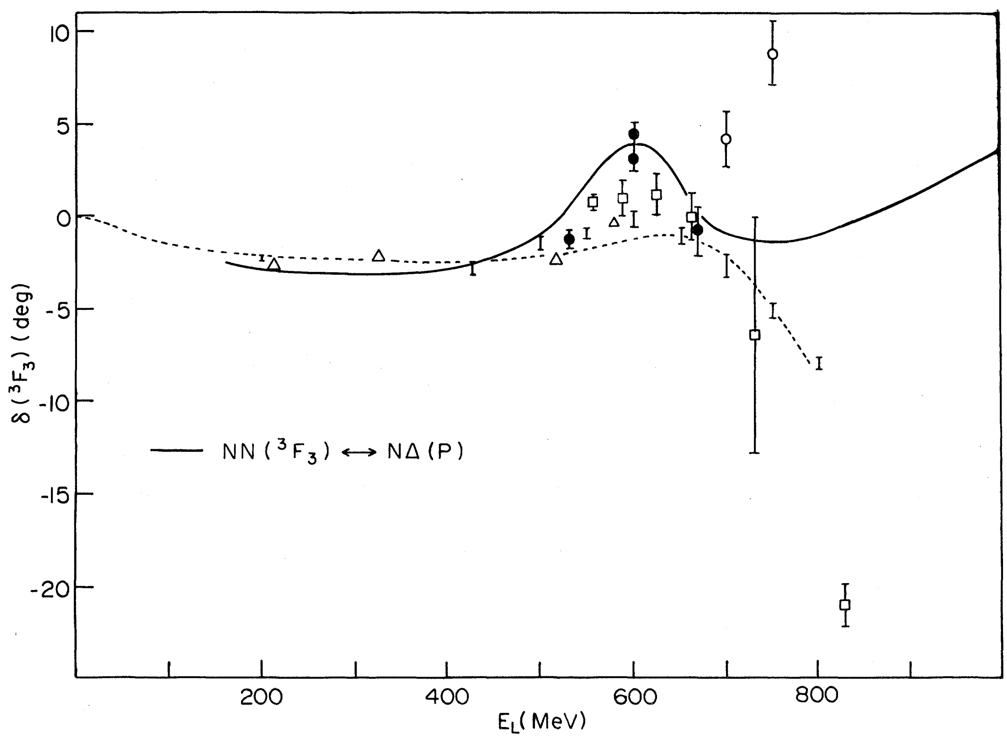

FIG. 2. The $^3F_3$ phase shift. The open triangles denote the 1980 phase-shift analyses of Ref. 29. The vertical bars denote the single-energy phase-shift analysis and the short-dashed curve the continuous-energy phase-shift analysis SM80 of Ref. 31. The open squares denote the analysis of Ref. 30. The filled circles denote solution 1 and the open circles solution 2 of Ref. 32. The solid curve is the model prediction for $NN(^3F_3)$ coupled to $N\Delta(P)$. The effect of the width $\Gamma_\Delta = 115.0$ MeV is included (the transition potential is consequently ignored). $f_{NN,NN} = 0.1$, $f_{NN,N\Delta} = 1.16$, $f_{N\Delta,N\Delta} = -0.4$.

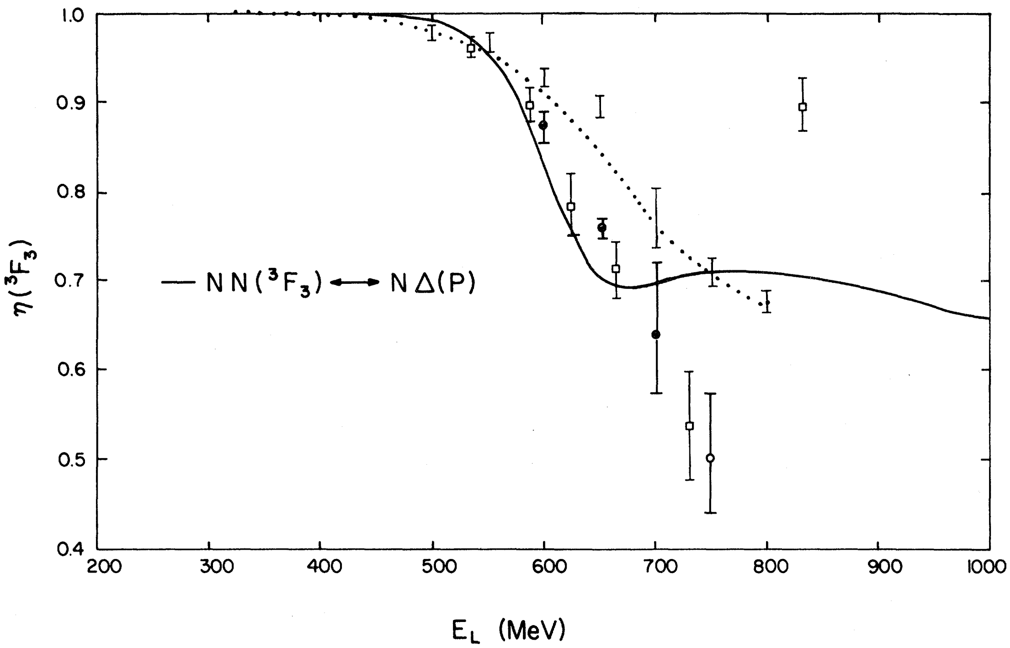

FIG. 3. The $^3F_3$ inelasticity. The points and curves denote phase-shift solutions and model predictions as in Fig. 2.

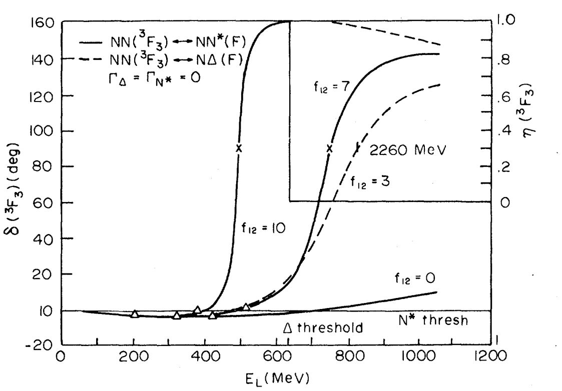

FIG. 4. The $^3F_3$ phase shift and inelasticity for several models coupling to F-wave isobar channels and without inclusion of the effect of isobar widths. The open triangles are the 1980 phase shifts of Ref. 29. Coupling to $N\Delta(F)$ with $f_{NN,NN}=1.29$, $f_{NN,N\Delta}=3.0$, and $f_{N\Delta,N\Delta}=0.0$ and $V_T=0$ is shown by the dashed curve. This fits δ for $E_L<515$ MeV and is a qualitative fit to the position and width of the structure of Ref. 3, but is too elastic. The solid curves represent coupling to $NN^*(1470)(F)$ showing the effect of increasing $f_{12}\equiv f_{NN,NN^*}$ from 0.0 to 10.0 as indicated beside the curves. $V_t=0$, $f_{NN^*,NN^*}=0.0$, and $f_{NN,NN}$ is adjusted so that $f_{\text{eff}}(0)=0.0$ [see, Eq. (22)] as in the case of coupling to $N\Delta(f)$. The phase shifts for $E_L \lesssim 325$ MeV are closely determined by $f_{\text{eff}}(0)$. The NN^* channel is closed for $E_L<1200$ MeV requiring that $\eta=1$.

tatively for the S matrix as it is known from the present data. Only the $^3F_2$ phase is clearly deficient.

A. The $^3F_3$ channel

We examine the $^3F_3$ channel first because it contains the most firmly established structure[3] as shown in Figs. 2 and 3. In addition to the model parameters expected to be dominant we discuss several other versions here to illustrate how the results depend in an essential way on the nature of the coupled channel. Because the $^3F_3$ channel is an $I=1$ state it can couple to the lowest-threshold isobar system, $N\Delta$. Furthermore it can couple to an $L'=1$, $N\Delta$ system, because the total spin can be as large as $S'=2$. We expect the $L'=3$ or 5 channels to be dominated by the $L'=1$ channels.

Figure 4 shows the results for coupling to either the $N\Delta$ or NN^* channels with $L'=3$ and vanishing resonance width. In both cases the resonance is too narrow and much too elastic. The high $NN^*(1470)$ threshold ($E_L=980$ MeV) makes the $^3F_3$ resonance completely elastic. Putting in the width of the isobars improves the prediction, but not sufficiently. Figure 5 shows the result of coupling to the expected channel, $N\Delta$ with $L'=1$, but with a vanishing isobar width. The results are now

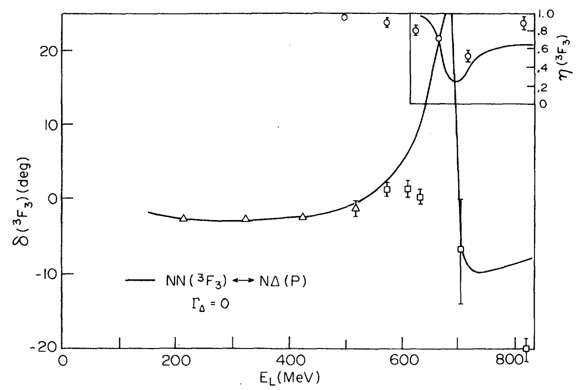

FIG. 5. The $^3F_3$ phase shift and inelasticity when coupled to $N\Delta(P)$ with no effect of isobar width. The solid curve is the model of Figs. 2 and 3 except that $\Gamma_\Delta=0$. The phase-shift analyses are denoted by points as in Fig. 2.

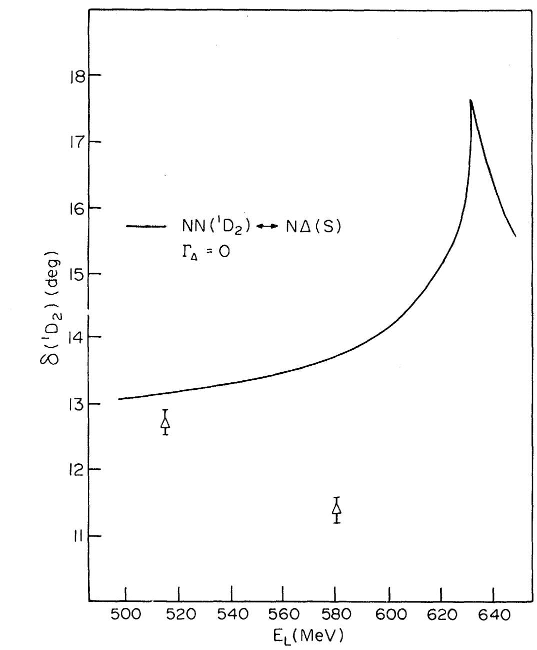

FIG. 6. The $^1D_2$ phase shift when coupled to $N\Delta(S)$ with $\Gamma_\Delta=0$. The cusp is at production threshold. The solid curve is the model for $V_T=0$, $f_{NN,NN}=5.19$, $f_{NN,N\Delta}=1.5$, $f_{N\Delta,N\Delta}=1.0$. The open triangles denote phase-shift solutions as in Fig. 2.

much more realistic, having about the correct width and inelasticity near resonance. However the phase-shift maximum, while it does not go through 90°, is too large, and the inelasticity is not sufficiently spread into the tails of the distribution.

Figures 2 and 3 show the best fit when $\Gamma_\Delta=115$ MeV is used. Given the uncertainties of the phase-shift analyses, it seems to be wholly adquate. The analyzed phase shifts are slightly lower at resonance than the model prediction, but this may be due to lack of sufficient experimental detail on the energy dependence. In this fit the choice of $f_{\Delta\Delta}\equiv f_{22}$ affected the shape of the real and imaginary parts of the phase shift near inelastic threshold, but could not change the resonance width or inelasticity by substantial amounts.

B. The $^1D_2$ channel

Because the $^1D_2$, NN channel can couple to the $N\Delta$ channel in an S wave, the effect is expected to be particularly strong. For $L'=0$ the values of ρ are large near threshold (see Appendix A) and a first-order cusp appears in the phase shift. As illustrated in Fig. 6 a moderate coupling strength, consistent with the increase of $\delta(^1D_2)$ up to $E_L=515$ MeV, produces a narrow (10-MeV wide) cusp at inelastic threshold, for zero-width Δ particles. Such a structure is not seen in the data. A weaker coupling giving too small a phase shift at 515 MeV will still give too large a result at 630 MeV.

However, as shown in Figs. 7 and 8, the situation is drastically changed when the actual width of the Δ is used. The cusp becomes "woolly" and a gentle rise of $\delta(^1D_2)$ is followed above threshold by a more rapid fall, and a substantial inelasticity is spread over several hundred MeV. This follows the general coupled-channel structure described in Sec. II and is not dependent upon the cusp. The fit to the data is good.

C. The $^3P_0$ channel

We next examine the $^3P_0$ channel because several of the phase shift analyses[29,31] have shown a slowing down of the rate of decrease of $\delta(^3P_0)$ near 515 MeV, and more recent analyses[30,31] indicate much inelasticity over a wide energy range. These experimental features are shown in Figs. 9 and 10. In the coupled-channel mechanism a large amount of inelasticity is associated with a resonant structure at or below inelastic threshold, which is 630 MeV in this case. The recent Arndt phase-shift analysis[31] indicates a shoulder in $\delta(^3P_0)$ in that energy region (see Fig. 9).

Indeed, increasing the coupling of $^3P_0$ to $N\Delta(L'=1)$ sufficiently to obtain the large inelasticities of the phase-shift analysis always induces

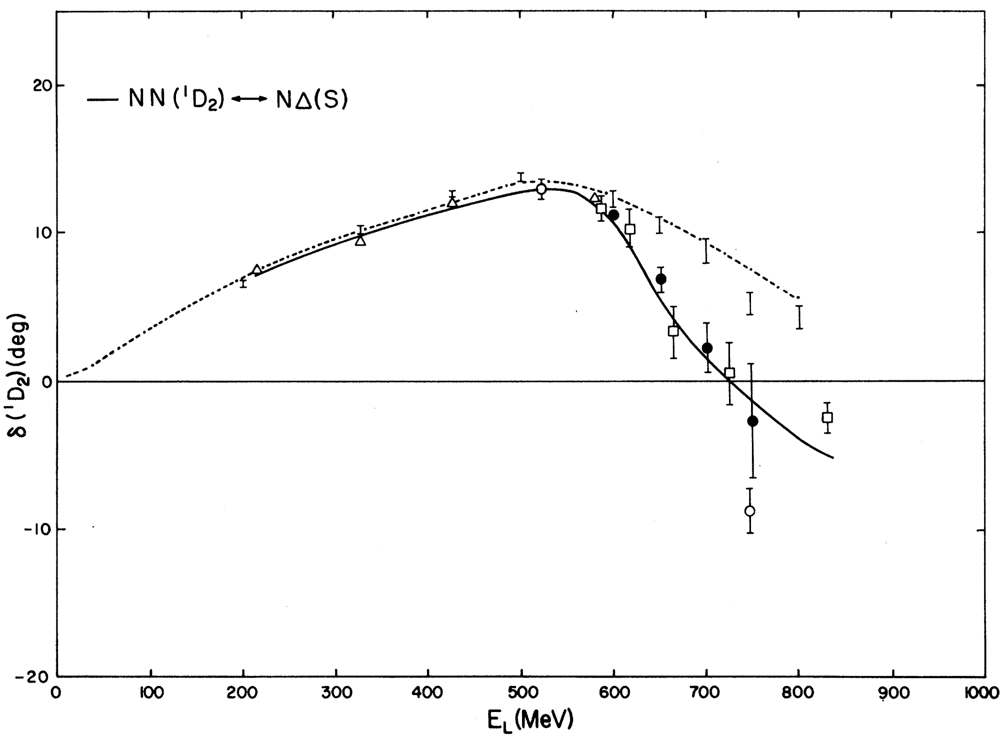

FIG. 7. The $^1D_2$ phase shift. The phase-shift analysis points and curve are denoted as in Fig. 2. The solid curve is the model prediction for $NN(^1D_2)$ coupled to $N\Delta(S)$, with $\Gamma_\Delta = 115.0$ MeV, $V_t = 0$, and $f_{NN,NN} = 10.34$, $f_{NN,N\Delta} = 3.279$, $f_{N\Delta,N\Delta} = 0.6$.

such a shoulder. The problem in this case is to keep $\eta(^3P_0)$ small over the large energy region, 515–800 MeV, indicated. Typically, as in the $^3F_3$ and $^1D_2$ case just examined, η has resonance shape and a width of about 100 MeV. The same is true in this case for two-channel fits. In order to better approximate the experimental inelasticity, a three-channel fit has been used: $NN(^3P_0)$ coupled to $N\Delta(P)$ and $NN^*(1440)(P)$. Figures 9 and 10 show the best fit obtained to the moderately and strongly inelastic phase-shift solutions. The fit to $\delta(^3P_0)$ is quite good. The prediction for the strongly inelas-

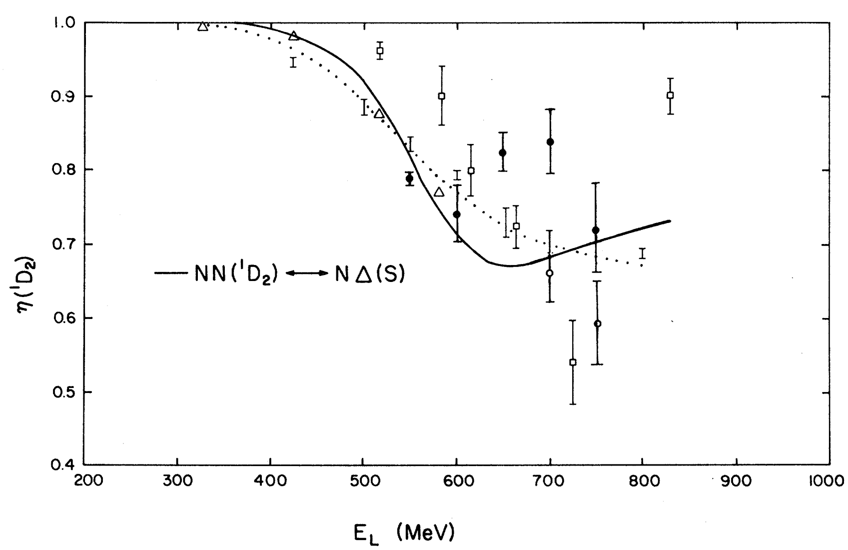

FIG. 8. The $^1D_2$ inelasticity. All points and curves are denoted as in Fig. 7.

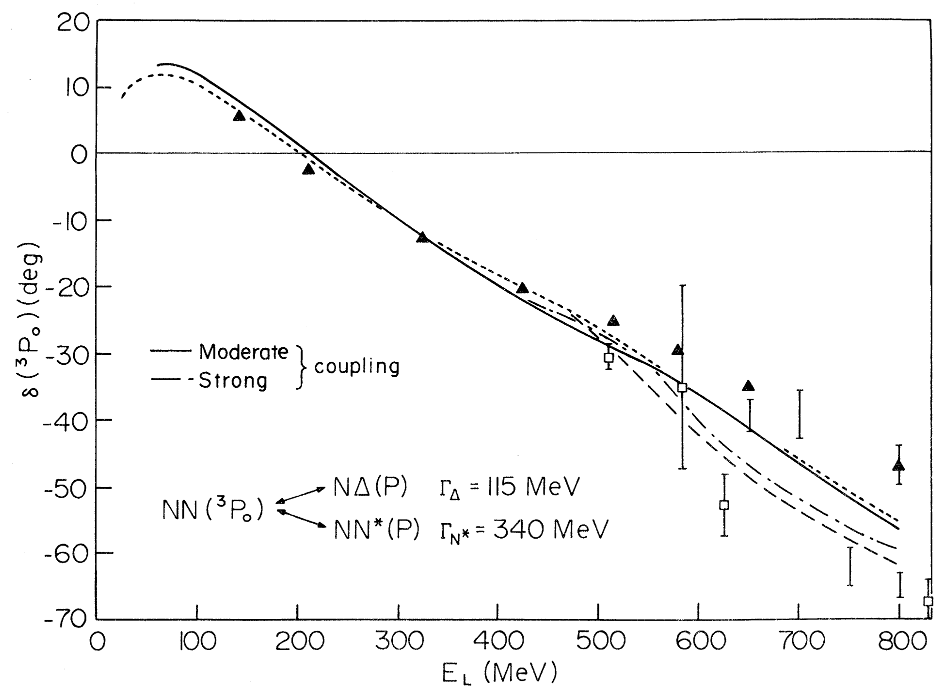

FIG. 9. The $^3P_0$ phase shift. The phase-shift-analysis points and short-dashed curve are denoted as in Fig. 2. The filled triangles are from the 1981 analysis of Ref. 29. The long-dashed curve is the continuous-energy analysis from SP81 of Ref. 31. The model curves correspond to $NN(^3P_0)$ coupled to $N\Delta(P)$ and $NN^*(1440)(P)$ with $\Gamma_\Delta=115.0$ MeV, $\Gamma_{N^*}=340.0$ MeV, and $V_T=0$. The solid curve corresponds to $f_{NN,NN}=44.0$, $f_{NN,N\Delta}=2.0$, $f_{NN,NN^*}=6.0$, $f_{N\Delta,N\Delta}=-0.7$, $f_{NN^*,NN^*}=-0.9$, and $f_{N\Delta,NN^*}=0.0$. The dash-dot curve corresponds to $f_{NN,NN}=83.0$, $f_{NN,N\Delta}=2.0$, $f_{NN,NN^*}=10.0$, $f_{N\Delta,N\Delta}=-0.7$, $f_{NN^*,NN^*}=-0.9$, $f_{N\Delta,NN^*}=0.0$.

tic $\eta(^3P_0)$ does not succeed in being small enough over the whole range, but is qualitatively adequate. The moderately inelastic values favored in the most recent analyses are fitted well. Long-range transition potentials may help in a fit to the strongly inelastic case, but the present numerical methods are inadequate to test that hypothesis with the necessarily nonvanishing Γ_Δ and Γ_{N^*}.

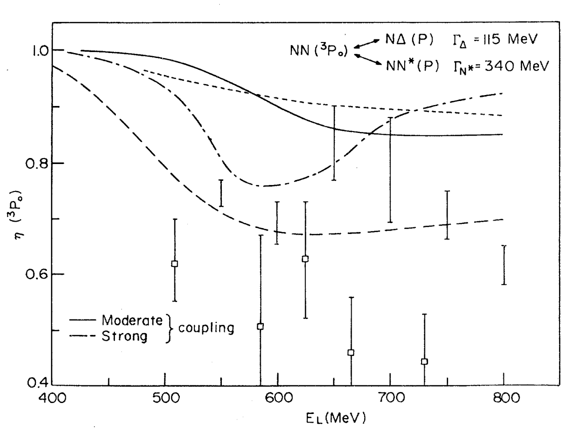

FIG. 10. The $^3P_0$ inelasticity. Points and curves are denoted as in Fig. 9. The 1981 analysis of Ref. 29 does not fit η, but takes $\eta\approx1$ from a theoretical calculation.

D. The $^1S_0$ channel

In this case it is not clear which coupled isobar channel is to be expected to dominate. Angular momentum selection rules prevent the $N\Delta$ channel (spin $S'=1$ or 2) from coupling to $J=0$ when $L'=0$. Therefore the lowest orbital angular momentum for the $N\Delta$ system is $L'=2$. The $NN^*(1440)$ system or the $\Delta\Delta$ system can couple to the $NN(^1S_0)$ channel, but their thresholds are 400 MeV higher (in laboratory energy). In the region $E_L<800$ MeV the extra orbital-angular-momentum barrier for $N\Delta$ is qualitatively similar in effect to the raised thresholds of the other channels. The result is (see Fig. 11) that either version of the model adequately fits $\delta(^1S_0)$. However the $NN^*(S)$ version (the $\Delta\Delta$ coupling would be very similar) fits the small $\eta(^1S_0)$ of the recent Arndt analysis[29] much better than coupling to $N\Delta$ system (Fig. 12). The $N\Delta(D)$ coupling version, on the other hand, is

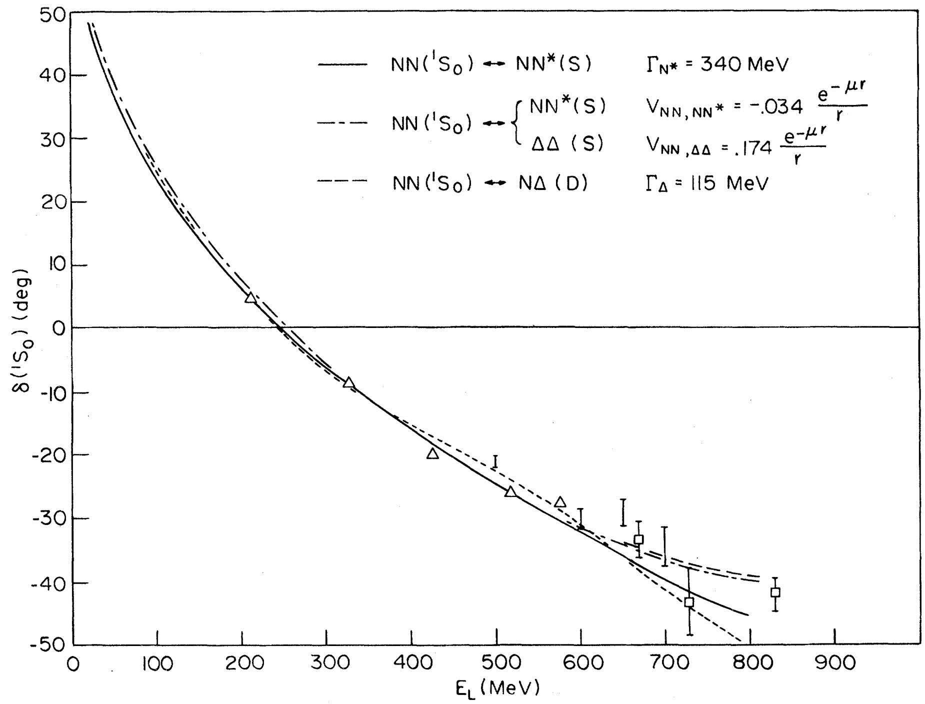

FIG. 11. The $^1S_0$ phase shift. The experimental points and short-dashed curve are denoted as in Fig. 2. The dash-dotted model curve represents $NN(^1S_0)$ coupled to $NN^*(1440)(S)$ and $\Delta\Delta(S)$ including coupling via the long-range OPE transition potential. $V_T(NN-NN^*)=-0.034r^{-1}e^{-\mu r}$, $V_T(NN-\Delta\Delta)=0.174r^{-1}e^{-\mu r}$, $f_{NN,NN}=3.67$, $f_{NN,NN^*}=2.4$, $f_{NN^*,NN^*}=0.5$, $f_{\Delta\Delta,\Delta\Delta}=0.5$, $f_{NN,\Delta\Delta}=f_{NN^*,\Delta\Delta}=0$, and $\Gamma_{N^*}=\Gamma_\Delta=0.0$. The solid curve represents $NN(^1S_0)$ coupled to $NN^*(1440)(S)$ with $\Gamma_{N^*}=340.0$ MeV, $V_T=0$, $f_{NN,NN}=3.4$, $f_{NN,NN^*}=2.3$, $f_{NN^*,NN^*}=0.5$. The long-dashed curve represents $NN(^1S_0)$ coupled to $N\Delta(D)$ with $\Gamma_\Delta=115.0$ MeV, $V_T=0$, $f_{NN,NN}=4.4$, $f_{NN,N\Delta}=2.8$, $f_{N\Delta,N\Delta}=0.5$.

consistent with the $\eta(^1S_0)\approx 1$ of Hoshizaki.[30] Recent data on D_{NN}, D_{SS}, and D_{SL} spin correlation coefficients for pp scattering of 800 MeV protons[33] strongly favor the Arndt solution.

Also shown in Fig. 11 is the effect of adding the one-pion-exchange NN-$\Delta\Delta$ and NN-NN^* transition potentials. The boundary-condition coupling is only slightly changed and the fit to $\delta(^1S_0)$ is very similar. However the predicted nn scattering length is much improved, becoming -15.6 fm instead of -12.6 fm.

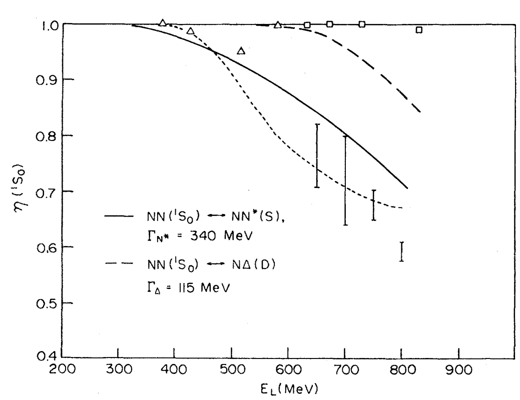

FIG. 12. The $^1S_0$ inelasticity. Points and curves are denoted as in Fig. 11.

E. The $^3P_1$ channel

The phase-shift analyses are fitted well by the elastic Feshbach-Lomon interaction for $E_L \leq 515$ MeV. In recent analyses small inelasticity is indicated for $E_L > 500$ MeV which implies a weak coupling, presumably to the $N\Delta(L'=1)$ channel. As shown in Fig. 13 this coupling is consistent with the inelasticity and the phase shifts up to $E_L = 800$ MeV. The one-pion-exchange potential does not alter the result significantly except in the threshold region where the Δ width is more important.

It has been suggested[34] that this channel may resonate at $E_L \approx 400$ MeV. In a recent paper[13] it has been shown that consistency with the available data and phase-shift analyses would require such a resonance, if it exists, to be very narrow ($\Gamma < 1$ MeV).

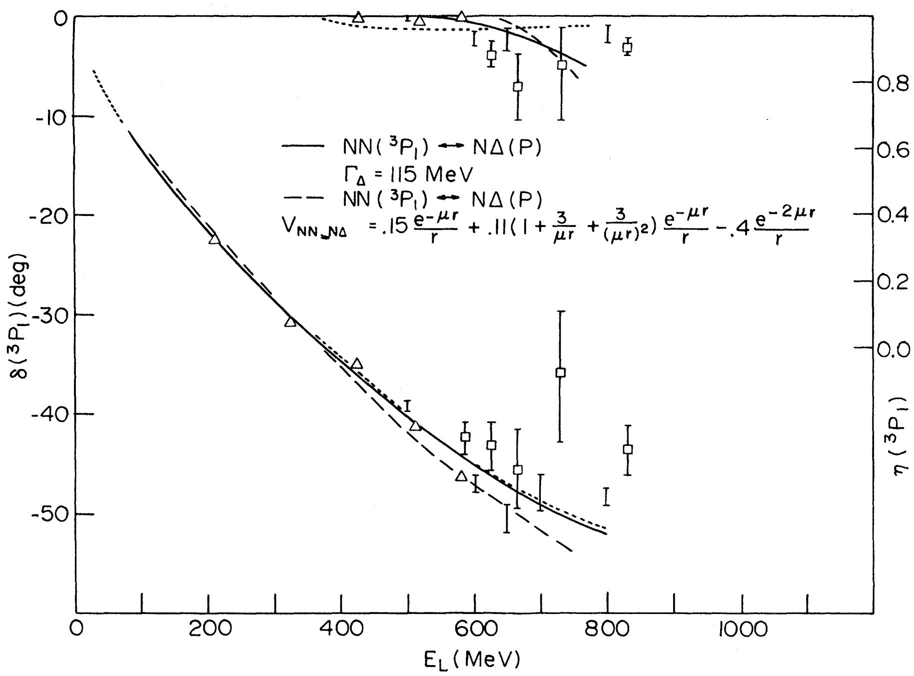

FIG. 13. The $^3P_1$ phase shift and inelasticity. The points and short-dashed curves denoted phase-shift solutions as in Fig. 2. The solid curve represents the model for $NN(^3P_1)$ coupled to $N\Delta(P)$ with $\Gamma_\Delta=115.0$ MeV and $V_T=0$, $f_{NN,NN}=22.1$, $f_{NN,N\Delta}=9.5$, and $f_{N\Delta,N\Delta}=4.0$. The long-dashed curve represents $NN(^3P_1)$ coupled to $N\Delta(P)$ taking the OPE transition potential into account, V_T is as described in the figure, $\Gamma_\Delta=0$, $f_{NN,NN}=40.0$, $f_{NN,N\Delta}=-2.0$, $f_{N\Delta,N\Delta}=1.0$.

F. The $^3P_2$-$^3F_2$ channels

The Feshbach-Lomon interaction[9] does not reproduce $\delta(^3F_2)$ well for $E_L>300$ MeV, as it remains positive and nearly constant while the data indicate a change of sign for $E_L\approx 500$ MeV. The potential in the $^3F_2$ state is attractive for large r. Although it becomes repulsive for $r<0.8$ fm, the orbital-angular-momentum barrier shields this effect (and that of the boundary condition) up to 700 MeV. The attraction in the $^3P_2$ channel comes from the core. Because of that it has little influence through the tensor potential on the $^3F_2$ state.

Long-range coupling of the $^3F_2$ state to an isobar state only increases the attraction at higher energies. Coupling the $N\Delta(L'=1)$ system to the $^3P_2$ channel does improve $\delta(^3P_2)$, ϵ_2, and the inelasticity parameters, as shown in Figs. 14 and 15 but has negligible influence on $\delta(^3F_2)$. The lack of fit of $\delta(^3F_2)$ is most likely to be ascribed to a deficiency of the semirelativistic nucleon-nucleon potential, for instance the neglect of spin-orbit and quadratic spin-orbit terms. This difficulty has little relevance to the validity of the coupled-channel mechanism.

G. The $^3F_4$-$^3H_4$ channels

These are satisfactorily described by the elastic Feshbach-Lomon interaction.[9] The boundary condition, which was not well determined by the low-energy data, was refitted to the intermediate-energy data. This results in a good fit to the data, as shown in Fig. 16 for $\delta(^3F_4)$ and ϵ_4. The $\delta(^3H_4)$ is essentially OPE and also agrees with the phase-shift analysis.

The analysis of Arndt[31] indicates that there may be a small inelasticity of the $^3F_4$ wave for $E_L>400$ MeV, but η remains greater than 0.995. This could easily be reproduced with a weak-to-moderate coupling to the $N\Delta$ channel, which can only couple for $L'\geq 3$, with negligible effect on the phase shifts or ϵ_4. The OPE transition potential will have little effect because of the large angular momentum barrier.

H. The $^3S_1$-$^3D_1$ channels

The Feshbach-Lomon-interaction fit to the $^3S_1$-$^3D_1$ tensor coupled channels is only satisfactory for

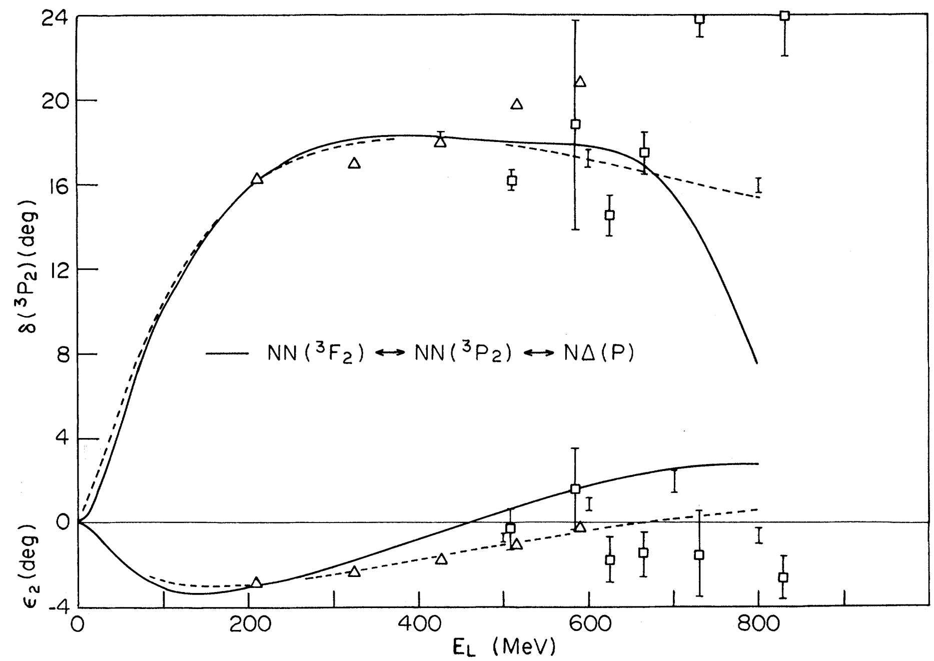

FIG. 14. The $^3P_2$ phase shift and the $J=2$ coupling parameter. The points and short-dashed curves denote phase-shift solutions as in Fig. 2. The solid curve represents the model in which the $NN(^3P_2)$ is coupled to $NN(^3F_2)$ via the NN tensor potential and to $N\Delta(P)$ via the core only. $\Gamma_\Delta=115.0$ MeV, $f_{P,P}=0.72$, $f_{P,F}=-0.9$, $f_{FF}=40.0$, $f_{P,N\Delta}=-0.9$, $f_{F,N\Delta}=f_{N\Delta,N\Delta}=0.0$.

$E_L \lesssim 210$ MeV. In comparison with the experimental phase shifts at 325–515 MeV the model $\delta(^3S_1)$ is slightly too repulsive; its $\delta(^3D_1)$ is approximately 10° too repulsive and its ϵ_1 changes signs at $E_L \approx 425$ MeV instead of remaining positive and increasing (see Figs. 17 and 18). Coupling the S-wave $NN^*(1440)$ channel or $\Delta\Delta$ channel decreases the repulsion in the $^3D_1$ channel as the energy increases. The change in the $^3D_1$ channel in turn improves ϵ_1 and $\delta(^3S_1)$.

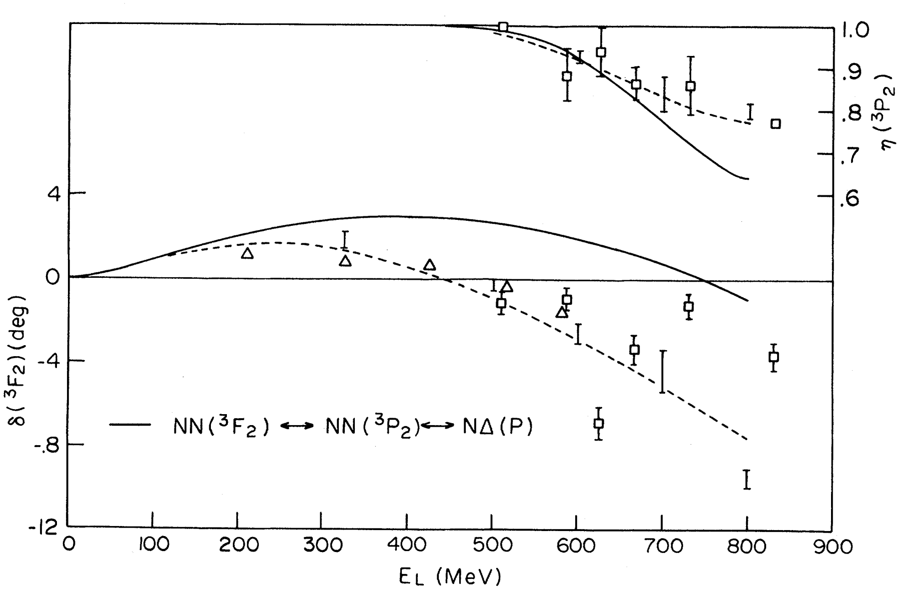

FIG. 15. The $^3F_2$ phase shift and the $^3P_2$ inelasticity. Inelastic, tensor coupled S-matrix parameters are as defined in Ref. 30. The imaginary coupling angle $\phi \le 3.5°$ and $\eta(^3F_2) \ge 0.999$. The points and curves are denoted as in Fig. 14.

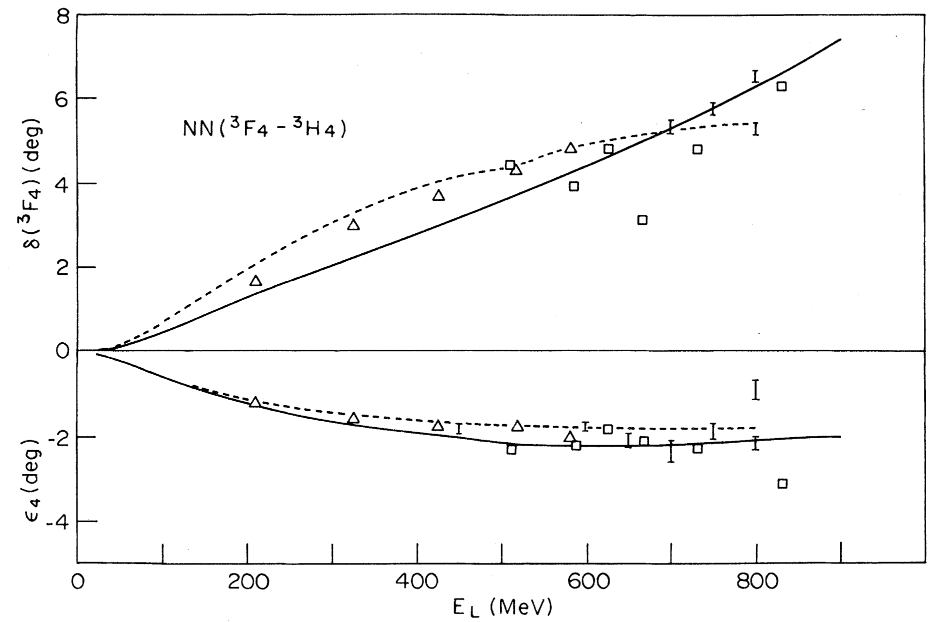

FIG. 16. The $^3F_4$ phase shift and the $J=4$ coupling parameter. The points and short-dashed curve denote phase-shift solutions as in Fig. 2, except that the Ref. 31 solution is WI80. The solid curve represents the Feshbach-Lomon interaction of Ref. 9 with no coupling to isobar channels and with $f_{FF}=0.8$, $f_{FH}=-2.0$, and $f_{HH}=25.0$.

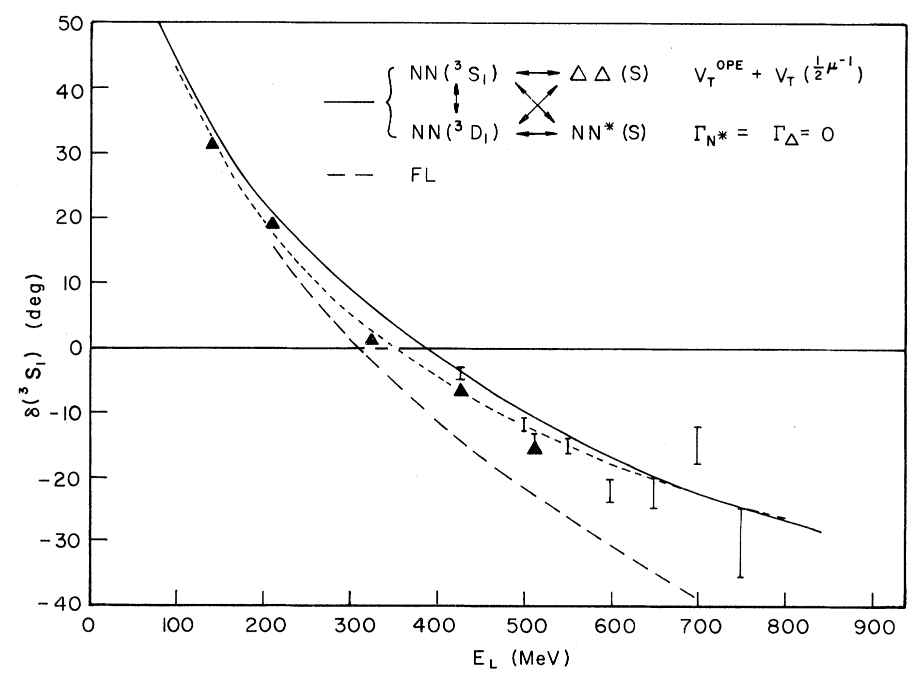

FIG. 17. The $^3S_1$ phase shift. The points and short-dashed curve denote phase-shift solutions as in Fig. 2 and the filled triangles denote the 1981 results of Ref. 29. The long-dashed curve represents the Feshbach-Lomon interaction, with no isobar channel coupling, with boundary condition parameters as given in Ref. 9 for the 5.2% D-state case. The solid curve is the model which includes the OPE coupling of $NN(^3S_1)$ and $NN(^3D_1)$ to the $\Delta\Delta(S)$ and $NN^*(1440)(S)$ channels, with $\Gamma_{N^*}=\Gamma_\Delta=0$, $f_{S,S}=5.9822$, $f_{S,D}=1.8$, $f_{D,D}=75.0$, $f_{S,\Delta\Delta}=2.4$, $f_{S,NN^*}=-3.2$, $f_{\Delta\Delta,\Delta\Delta}=1.0$, $f_{NN^*,NN^*}=2.0$, and $f_{D,\Delta\Delta}=f_{D,NN^*}=f_{\Delta\Delta,NN^*}=0.0$. The V_T are given in the text.

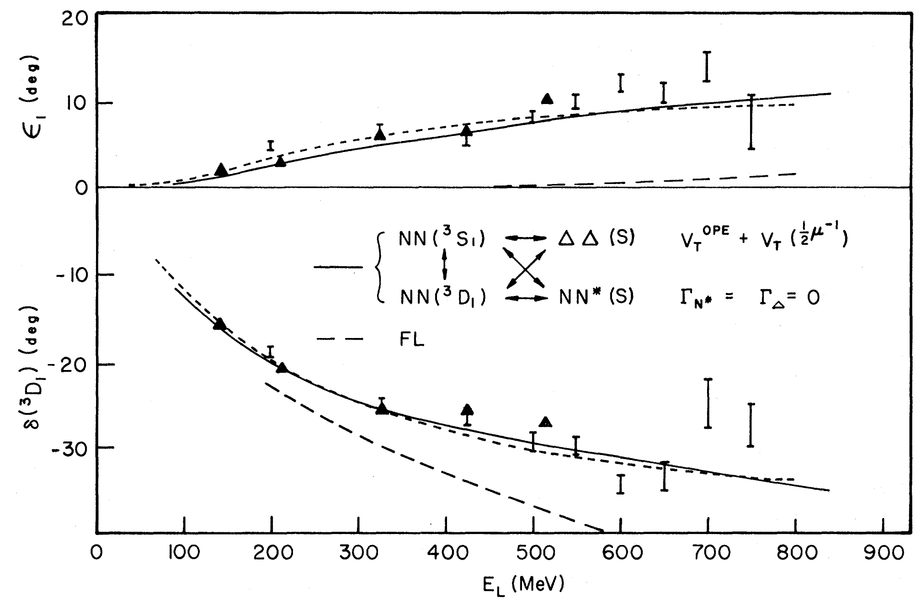

FIG. 18. The $^3D_1$ phase shift and the $J=1$ coupling parameter. The points and curves denote phase-shift and model solutions as in Fig. 17.

All attempts to fit $\delta(^3D_1)$ with only boundary-condition coupling to the isobar channel failed to be effective enough at 325 MeV when it had already overcorrected at 515 MeV. In addition the strong repulsion in the $^3D_1$ state at the core shielded ϵ_1 and $\delta(^3S_1)$ from the shift of $\delta(^3D_1)$. A further addition of isobar-channel coupling directly to the $^3S_1$ channel did not alter ϵ_1 properly.

The results improved greatly when the OPE and a $\frac{1}{2}\mu^{-1}$ range Yukawa potential were used to couple $NN(^3S_1)$ and $NN(^3D_1)$ with $\Delta\Delta$ and with $NN^*(1470)$ in an S wave:

$$V_T[NN(^3S_1)\text{-}\Delta\Delta(^3S_1)] = 0.174\mu V_0(\mu r) + 2.4 r^{-1} e^{-2\mu r} ,$$

$$V_T[NN(^3D_1)\text{-}\Delta\Delta(^3S_1)] = -0.11\mu V_2(\mu r) + 0.1 r^{-1} e^{-2\mu r} ,$$

$$V_T[NN(^3S_1)\text{-}NN^*(^3S_1)] = -0.034\mu V_0(\mu r) - 0.7 r^{-1} e^{-2\mu r} ,$$

$$V_T[NN(^3D_1)\text{-}NN^*(^3S_1)] = -0.096\mu V_2(\mu r) .$$

As can be seen in Figs. 17 and 18 the fit is now good for the whole energy range for the δ's and ϵ. Also $a_t = 5.413$ fm, in agreement with experiment. We cannot make a quantitative prediction for the inelasticity because of the technical limitation of our coupled-channel calculation which is unable to include the nonvanishing width of the isobars at the same time as using a transition potential tail. Therefore below the threshold for the central mass of $N^*(1440)$ or the Δ which are above our energy range, $\eta(^3S_1) = \eta(^3D_1) = 1$. In Arndt's analysis[31] the minima of $\eta(^3S_1)$ and $\eta(^3D_1)$ are 0.94 and 0.97, respectively, at $E_L = 425$ MeV but the Bugg analysis[29] obtains an adequate fit at that energy with completely elastic $I=0$ channels. Within the uncertainties of the present data a nearly elastic $^3S_1$-$^3D_1$ fit is a possibility, and the phase-shift fits may not be greatly perturbed when it is possible to include the width of the isobar for this case.

I. The $^1P_1$ channel

The elastic Feshbach-Lomon interaction is a poor representation of the $^1P_1$ partial wave even at comparatively low energies (see Ref. 9). The potential is strongly repulsive and requires a very strongly attractive core to compensate. This combination does not give the correct energy dependence. The prediction is too repulsive for $E_L < 100$ MeV and is too attractive for $E_L > 300$ MeV.

Coupling to an $NN^*(1440)$, $L'=1$ state improves the results markedly. Normally, as in all other cases discussed here, coupling to the isobar channel would cause an attraction increasing with energy. The reverse effect is desired and indeed is obtained in this case because of the strongly nonmonotonic interaction of the diagonal NN interaction. The attraction due to the interchannel coupling allows a drastic reduction of the attraction of the core in the diagonal interaction. The effect of the core increases sharply with energy and this energy dependence dominates providing that the transition potential is of longer range than the core. The reduction is core attraction therefore corrects the energy dependence.

Both $V_T=1.7r^{-1}\exp(-\mu r)$ and $V_T=3.0r^{-1}\times\exp(-2\mu r)$ give moderate fits as shown in Fig. 19. The longer-range potential is better at low energies,[35] and the shorter-range potential is better at higher energies [although there is ambiguity in the phase-shift results at 650 MeV (Ref. 31)]. This suggests a mixture of one- and two-pion range transition potentials, and the possibility that OPE predictions supplemented by a phenomenological $\frac{1}{2}\mu^{-1}$ transition potential may represent the data.

From Eqs. (13) and (15) we obtain

$$V_T[NN(^1P_1)\text{-}NN^*(^1P_1)]=0.1\mu V_0(\mu r)\ ,$$

$$V_T[NN(^1P_1)\text{-}\Delta\Delta(^1P_1)]=0.23\mu V_0(\mu r)\ ,$$

and

$$V_T[NN(^1P_1)\text{-}\Delta\Delta(^5P_1)]=-0.15\mu V_2(\mu r)\ .$$

Because of the factor $[1+3(\mu r)^{-1}+3(\mu r)^{-2}]$ in $V_2(\mu r)$ the OPE coupling to the $\Delta\Delta(^5P_1)$ channel is much stronger than that to the $\Delta\Delta(^1P_1)$ channel. In light of this the computation was simplified to a three-channel problem by approximately including the effect of the $\Delta(^1P_1)$ coupling in the transition interaction to the $\Delta\Delta(^5P_1)$ channel. Examination of Eq. (9) shows that the effective strength of several channels i coupled to the NN channel by V_T^i is

$$V_T^{\text{eff}}=\left[\sum_i (V_T^i)^2\right]^{1/2} . \tag{31}$$

In the present case $V_T^{\Delta\Delta}(^1P_1)\ll V_T^{\Delta\Delta}(^5P_1)$ and we may approximate

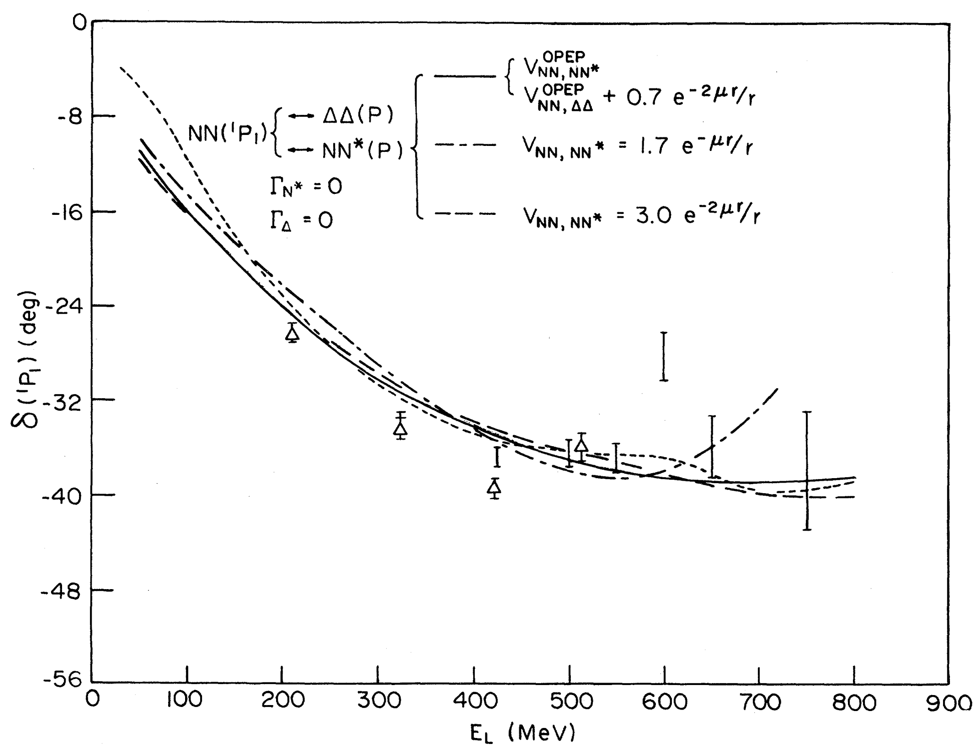

FIG. 19. The $^1P_1$ phase shift. The points and short-dashed curve denote phase shifts as in Fig. 2. The solid curve represents the model with the OPE coupling of $NN(^1P_1)$ to $NN^*(1440)(^1P_1)$, $\Delta\Delta(^1P_1)$, and $\Delta\Delta(^5P_1)$, and a $\frac{1}{2}\mu^{-1}$ range coupling to $\Delta\Delta(P)$ as described in the text; and $f_{NN,NN}=3.0$, $f_{NN,NN^*}=3.13$, $f_{NN^*NN^*}=2.0$, $f_{\Delta\Delta,\Delta\Delta}=1.0$, and $f_{NN,\Delta\Delta}=f_{NN^*,\Delta\Delta}=0.0$. The dash-dotted and long-dashed curves represent the best fit with, respectively, μ^{-1} and $\frac{1}{2}\mu^{-1}$ range transition potentials to the $NN^*(P)$ channel only, with coefficients given in the figure and the text. For the μ^{-1} case $f_{NN,NN}=150.0$, $f_{NN,NN^*}=23.0$ $f_{NN^*,NN^*}=2.0$. For the $\frac{1}{2}\mu^{-1}$ case $f_{NN,NN}=3.5$, $f_{NN,NN^*}=2.5$, and $f_{NN^*,NN^*}=2.0$.

$$V_T^{\text{eff}}=[V_T{}^2({}^5P_1)+V_T{}^2({}^1P_1)]^{1/2}\approx V_T({}^5P_1)+\left[\frac{1}{2}\frac{V_T({}^1P_1)}{V_T({}^5P_1)}\right]V_T({}^1P_1)\ .$$

Using $\mu r=3$ as an average position to evaluate the coefficient in square brackets we obtain

$$V_T^{\text{eff}}(NN\text{-}\Delta\Delta)=V_T^{\Delta\Delta}({}^5P_1)-0.33V_T^{\Delta\Delta}({}^1P_1)\ .$$

Using this, the above OPE NN-NN^* transition potential, and a phenomenological shorter-range transition potential to the $\Delta\Delta$ channel,

$$Ar^{-1}e^{-2\mu r}\ ,$$

we obtain a best fit with $A=0.7$, shown in Fig. 19.

In this case the use of the theoretical long-range potential improves the results obtained with phenomenological potentials of a single range. The Arndt analysis[31] predicts a small inelasticity at higher energies, but again we are prevented by technical difficulties from putting $\Gamma_{N^*}\neq 0$ to predict the inelasticity.

J. The ${}^3D_2$ channel

The ${}^3D_2$ phase shifts of Refs. 29 and 31 are reasonably well fitted by the uncoupled Feshbach-Lomon (FL) model.[9] However, the OPE transition potentials alone are significant. Furthermore, the phase shifts of Ref. 30 hint at a structure for $E_L\approx 625$ MeV. Therefore it is of interest to examine the effects of channel coupling.

The OPE predictions are

$$V_T[NN({}^3D_2)\text{-}NN^*({}^3D_2)]=-0.034\mu V_0(\mu r)-0.068\mu V_2(\mu r)\ ,$$

$$V_T[NN({}^3D_2)\text{-}\Delta\Delta({}^3D_2)]=0.17\mu V_0(\mu r)+0.0034\mu V_2(\mu r)\ ,$$

$$V_T[NN({}^3D_2)\text{-}\Delta\Delta({}^7D_2)]=0.023\mu V_2(\mu r)\ .$$

In this case the potential coupling to the $\Delta\Delta({}^7D_2)$ channel is much weaker than that to the $NN^*({}^3D_2)$ channel. We therefore quadratically add the effect of the former to V_2 in the latter using Eq. (31), obtaining

$$V_T^{\text{eff}}[NN({}^3D_2)\text{-}NN^*(D)]=-0.034\mu V_0(\mu r)-0.071\mu V_2(\mu r)$$

reducing the case to a three-channel problem.

By varying the $\frac{1}{2}\mu^{-1}$ range transition potentials and the core boundary condition we can then get the two types of fit shown in Fig. 20. Both predict phase shifts which are a little too large for $E_L=200-300$ MeV (the uncoupled FL potential is better at these energies). The fit with moderate core coupling fits the phases of Ref. 31 well at higher energies. Strong core coupling improves the fit at the lower energies and qualitatively fits the structure of Ref. 30 at higher energies.

K. The ${}^3D_3$-${}^3G_3$ channels

Again the predictions of the FL interaction[9] are a moderately good fit to the phase shifts of Refs. 29 and 31. The OPE transition potential situation is complicated by the number of channels, predicting

$$V_T[NN({}^3D_3)\text{-}NN^*({}^3D_3)]=-0.034\mu V_0(\mu r)+0.0194\mu V_2(\mu r)\ ,$$

$$V_T[NN({}^3G_3)\text{-}NN^*({}^3D_3)]=-0.101\mu V_2(\mu r)\ ,$$

$$V_T[NN({}^3D_3)\text{-}\Delta\Delta({}^7S_3)]=-0.181\mu V_2(\mu r)\ ,$$

$$V_T[NN({}^3D_3)\text{-}\Delta\Delta({}^3D_3)]=0.174\mu V_0(\mu r)+0.010\mu V_2(\mu r)\ ,$$

$$V_T[NN({}^3G_3)\text{-}\Delta\Delta({}^3D_3)]=0.174\mu V_0(\mu r)-0.063\mu V_2(\mu r)\ ,$$

$$V_T[NN({}^3D_3)\text{-}\Delta\Delta({}^7D_3)]=-0.310\mu V_2(\mu r)\ ,$$

$$V_T[NN({}^3G_3)\text{-}\Delta\Delta({}^7D_3)]=0.257\mu V_2(\mu r)\ .$$

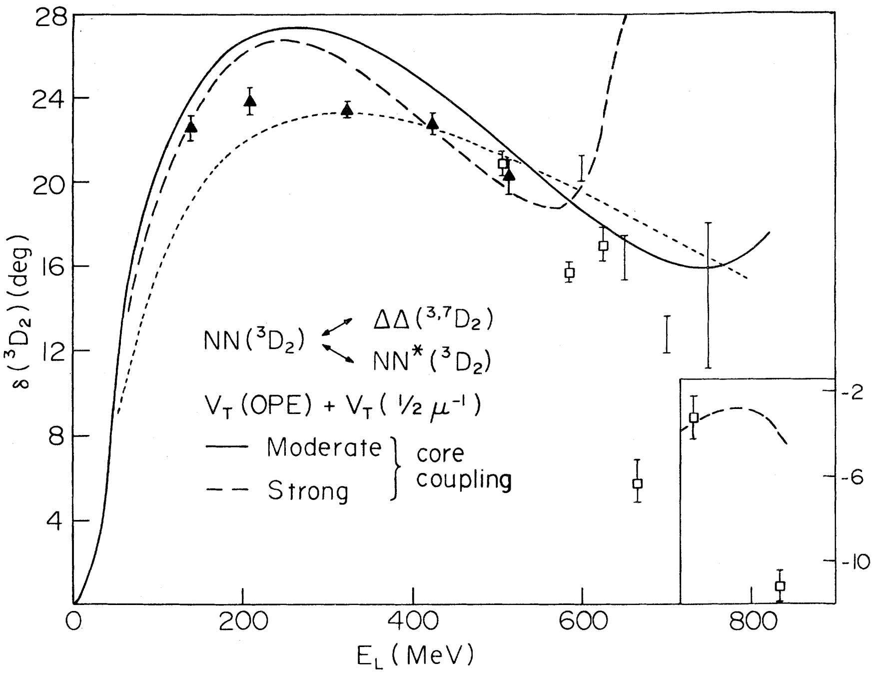

FIG. 20. The $^3D_2$ phase shift. The points denote phase-shift solutions as in Figs. 2 and 9 except for the vertical bars, which like the short-dashed curve denote the SF81 solutions (single and continuous energy, respectively) of Ref. 31. The solid and long-dashed curves represent the model prediction for $NN(^3D_2)$ coupled to $NN^*(^3D_2)$, $\Delta\Delta(^3D_2)$, and $\Delta\Delta(^7D_2)$ through OPE transition potentials described in the text. In addition they have transition potentials $r^{-1}e^{-2\mu r}$ with coefficients of 0.5 for coupling to NN^* and -0.4 for coupling to $\Delta\Delta$. The solid curve is determined by $f_{NN,NN}=157.0$, $f_{NN,NN^*}=-12.0$, $f_{NN,\Delta\Delta}=20.0$, $f_{NN^*NN^*}=1.0$, $f_{\Delta\Delta,\Delta\Delta}=1.0$, and $f_{NN^*,\Delta\Delta}=0.0$. The long-dashed curve is determined by $f_{NN,NN}=5230.0$, $f_{NN,NN^*}=-100.0$, $f_{NN,\Delta\Delta}=100.0$, $f_{NN^*,NN^*}=1.0$, $f_{\Delta\Delta,\Delta\Delta}=1.0$, and $f_{NN^*,\Delta\Delta}=0$.

Couplings to other $\Delta\Delta(S)$ or $\Delta\Delta(D)$ states vanish. Nevertheless this case is in principle a six-channel problem. Only the S-wave and the D-wave isobar channels behave in significantly different ways and we approximate the total effect well by combining all of the V_2-type coupling to $NN^*(D)$ and $\Delta\Delta(D)$ channels through Eq. (31). The V_0 potentials in the coupling to $\Delta\Delta(^3D_3)$ are weaker than the V_2 potentials and have opposite relative signs, so we ignore them. We obtain

$$V_T^{\rm eff}[NN(^3D_3)\text{-}\Delta\Delta(D)]=-0.311\mu V_2(\mu r)\ ,$$

$$V_T^{\rm eff}[NN(^3G_3)\text{-}\Delta\Delta(D)]=0.283\mu V_2(\mu r)$$

while $V_T[NN(^3D_3)\text{-}\Delta\Delta(^7S_3)]$ is as above.

As shown in Fig. 21, after varying $V_T(\frac{1}{2}\mu^{-1})$ and the core, fits to the δ's and ϵ_3 of Ref. 31 are very good. The values of $\delta(^3D_3)$ of Ref. 29 are lower for $E_L=325$ MeV, 425 MeV, and 515 MeV.

L. The $^1F_3$ channel

The phase-shift solutions of Refs. 29 and 31 show a smooth, elastic behavior for the $^1F_3$ channel but recent $\Delta\sigma_L$ data from protons on deuterons[3] indicate energy dependence in the $I=0$ channel. This is incorporated into the analysis of Hoshizaki,[30] who obtains a resonantlike effect near $E_L=650$ MeV and significant inelasticity. We examine the fit to both the smooth and the structured behavior.

The $\Delta\Delta(^5P_3)$ channel can couple to the $NN(^1F_3)$. The other $\Delta\Delta$ and the NN^* channels can only couple for $L'\geq 3$ which makes them unimportant in our energy range. Hence we need only use the OPE,

$$V_T[NN(^1F_3)\text{-}\Delta\Delta(^5P_3)]=-0.118\mu V_2(\mu r)\ .$$

To obtain a fit to the smooth phase shifts[29,31] one must reduce the strong effect of the above OPE transition potential. This is accomplished by adding a $\frac{1}{2}\mu^{-1}$ range transition potential and a core boundary condition of opposite sign. One then obtains the good fit shown in Fig. 22. The fit with no coupling[9] is poor, as it decreases with energy too quickly for $E_L>300$ MeV.

Because of the importance of the inelasticity

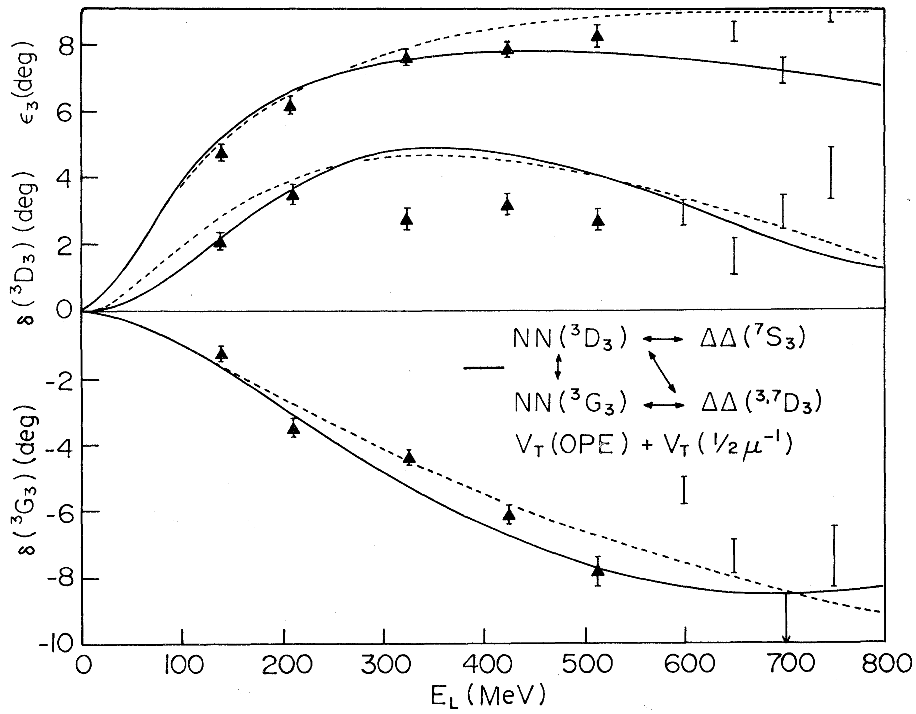

FIG. 21. The $^3D_3$ and $^3G_3$ phase shifts and the $J=3$ coupling parameter. The points and short-dashed curve denote phase-shift solutions as in Fig. 20. The solid curve describes the $NN(^3D_3)$ and $NN(^3G_3)$ channels coupled to $\Delta\Delta(^7S_3)$, $\Delta\Delta(^3D_3)$, $\Delta\Delta(^7D_3)$, and $NN^*(^3D_3)$ via the OPE transition potential described in the text and also with transition potentials $r^{-1}e^{-2\mu r}$ with coefficients of 1.6, 2.9, and -1.3 for the $NN(^3D_3)$ to $\Delta\Delta(^7S_3)$, for the $NN(^3D_3)$ to $\Delta\Delta(D)$ and for the $NN(^3G_3)$ to $\Delta\Delta(D)$, respectively. The core parameters are $f_{D,D}=57.0$, $f_{D,G}=-3.5$, $f_{G,G}=0.7$, $f_{D,\Delta\Delta(S)}=-8.0$, $f_{D,\Delta\Delta(D)}=-0.4$, $f_{G,\Delta\Delta(D)}=-0.5$, $f_{\Delta\Delta(S),\Delta\Delta(S)}=1.0$, $f_{\Delta\Delta(D),\Delta\Delta(D)}=0.1$, $f_{D,\Delta\Delta(S)}=f_{\Delta\Delta(S),\Delta\Delta(D)}=0$.

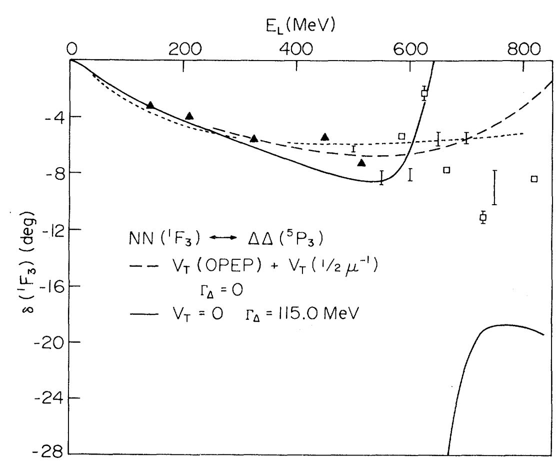

FIG. 22. The $^1F_3$ phase shift. The phase-shift solutions are denoted as in Fig. 20. The long-dashed curve represents the model for $NN(^1F_3)$ coupled to $\Delta\Delta(^5P_3)$ with an OPE transition potential $-0.12V_2(\mu r)$ plus the shorter-range transition potential $1.7r^{-1}e^{-2\mu r}$, $\Gamma_\Delta=0$, $f_{NN,NN}=-2.15$, $f_{NN,\Delta\Delta}=0.4$, and $f_{\Delta\Delta,\Delta\Delta}=1.0$. The solid curve represents core coupling between the same channels with $\Gamma_\Delta=115.0$ MeV, $f_{NN,NN}=50.0$, $f_{NN,\Delta\Delta}=-14.09$, and $f_{\Delta\Delta,\Delta\Delta}=1.0$.

in the resonant solution, we include the width $\Gamma_\Delta=115.0$ MeV and must ignore the transition potential tail. Adjusting the core boundary condition we obtain the fit of Figs. 22 and 23. The data fit of Ref. 30 has a much narrower width $\delta(^1F_3)$ structure than its $\eta(^1F_3)$ structure. This is inconsistent with a true resonance. Our resonant-model fit is a compromise between fitting the energy dependence of the δ and the η of Ref. 30.

VI. CONCLUSIONS

We have shown that the coupling of isobar channels to the nucleon-nucleon channels provides a natural explanation for the observed $^1D_2$ and $^3F_3$ structures and the possible $^3P_0$ structure. Although core parameters are adjusted to fit the position of a resonance, the model itself determines the width and inelasticity of the resonance.

The Argand diagrams for these three channels are given in Figs. 24–26 to illustrate the degree of "resonance" of the model and phase-shift-analysis results. In Fig. 24 one of the model solutions

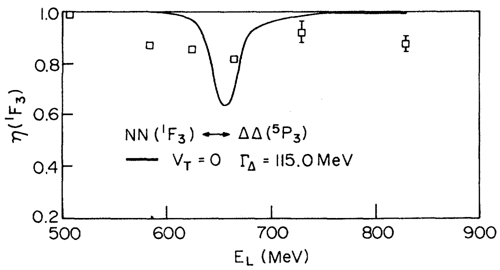

FIG. 23. The $^1F_3$ inelasticity. The phase-shift solution and the model curve are denoted as in Fig. 22.

shows a distinct counterclockwise motion for $E_L = 515-700$ MeV. In this same region one of the energy-dependent phase-shift solutions[31] is a straight section between clockwise-turning behavior at lower and higher energies.

Other investigations[20,21] of the $^1D_2$ and $^3F_3$ coupling to the $N\Delta$ channel agree that resonantlike structure in the sense of counterclockwise rotation in the Argand plot is produced by coupled channels. However there is uncertainty and disagreement as to the presence of poles in the complex energy plane corresponding to the resonances. The

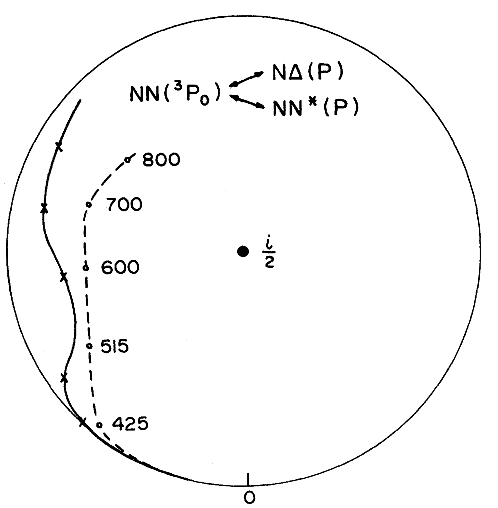

FIG. 24. Argand plot for the $^3P_0$ amplitude. The dashed curve denotes the phase-shift solutions SM80 of Ref. 31. The solid curve represents the model for $NN(^3P_0)$ core coupled to $N\Delta(P)$ and $NN^*(1470)(P)$. $\Gamma\Delta = 115.0$ MeV, $\Gamma_{N^*} = 200.0$ MeV, $f_{NN,NN} = 111.0$, $f_{NN,N\Delta} = 3.0$, $f_{NN,NN^*} = 12.0$, $f_{NN^*,NN^*} = -0.9$, $f_{N\Delta,NN^*} = 0.0$. The crosses on the model denote the same energies as the circles on the phase-shift analysis curve. The laboratory energies E_L are indicated in MeV.

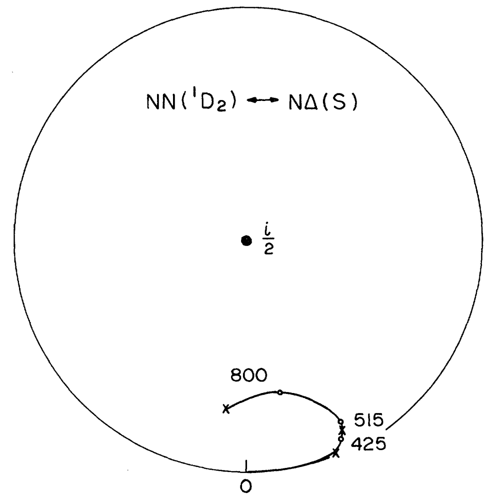

FIG. 25. Argand plot for the $^1D_2$ amplitude. The SM80 phase shifts fall on top of the model curve (the same model as in Fig. 7). Energy positions are denoted as in Fig. 24.

more analytic discussions of coupled-channel behavior[8,21(a)] find associated poles, although sometimes at a great distance. In those models where a numerical search for poles is required[20,21(b)] they are often not found.

Furthermore, we have shown that if the coupled-channel mechanism is used together with the Feshbach-Lomon interaction as the diagonal NN interaction that, for $E_L \leq 800$, one can fit all phases for $L \leq 3$, with the exception of $\delta(^3F_2)$. For

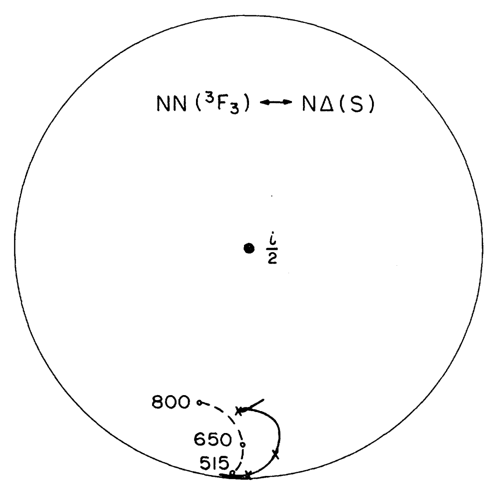

FIG. 26. Argand plot for the $^3F_3$ amplitude. The dashed curve denotes the S80 phase shifts of Ref. 31. The solid curve represents the model of Fig. 2. Energy positions are denoted as in Fig. 24.

$L > 3$ one must have $L' \geq 2$ for the lowest-threshold ($N\Delta$) channel, so that coupling effects are expected to be weaker in the present energy range. Other observed structures are at higher energy than we have explored.

The deficiency of the model for the $^3F_2$ phase shift can more likely be ascribed to the semirelativistic Feshbach-Lomon potential than to the coupled-channel mechanism. The inability to obtain the very large $^3P_0$ inelasticity of the earlier Arndt analysis[31] may be moot due to the smaller inelasticity of more recent analyses, but one may get more inelasticity on overcoming the inability to calculate with long-range transition potentials when the widths of the isobars are taken into account. Because of the same technical limitation we were not able to examine the effect of long-range potential in channels where inelasticity was important and we have not predicted the small inelasticity of some channels where it was essential to use long-range transition interactions.

Although we did not set out at this stage to use theoretical transition potentials, we have in fact shown consistency with the one-pion-exchange calculations. Furthermore, in the $^3S_1$-$^3D_1$, $^1S_0$, and $^1P_1$ channels, the one-pion-exchange potential provides a definite improvement in the fit to the data.

The major physical question remains as to whether the core is adequately described by an energy-independent boundary condition. If the boundary condition has strong energy dependence, that can cause resonances or otherwise modify the phase-shift behavior in a major way. The existence of bound or resonant states of the underlying six-quark system will in fact introduce poles on the real energy axis into the f matrix.[36]

In the bag model the states of the system are completely confined and the resulting S-matrix poles are at real energies. However the physical color-singlet pairs are not confined as in the bag model. When this is taken into account one may expect large movements of the S-matrix poles. On the other hand as Jaffe and Low have pointed out[36] the f-matrix pole calculated at the confinement radius does not move, because the zero of the wave function at the confinement radius remains fixed when the confinement is removed.

Unless the residues of the f-matrix poles are small the related S-matrix pole may be far away in energy from the f-pole position. Furthermore, the S-matrix pole may be far from the real axis and even on a different sheet.[8,36] Therefore, in principle one does not expect the experimental structures to coincide with the six-quark states. A comparison of the predicted six-quark bag states[5,6] with the data shows that the relation is not direct[7]: (i) the experimental states are, on average, several hundred MeV lower than the bag states; (ii) the energy shift is not uniform, in particular the degenerate experimental states are 80 MeV and 130 MeV apart in the bag-state spectrum; (iii) the bag spectrum is an order of magnitude denser than the states so far observed; and (iv) widths and inelasticities of the structures are, at best, only qualitatively predicted by the bag model. Although corrections to the S-matrix pole distributions have been discussed qualitatively[6] no quantitative description has been proposed without reference to the f matrix.

When the long-range interaction in the form of the Paris potential[2] is taken into account[7] the internally (bag state) and externally (phase shifts and long-range interaction) determined f-matrix poles agree well with each other for the $^1S_0$ and the $^3S_1$-$^3D_1$ states, at $E_L = 795$ and 607 MeV, respectively, although the physical S-matrix poles are over 600 MeV lower. When the coupled-channel interaction of this paper is used the $^3S_1$-$^3D_1$ f-matrix poles agree excellently. The $^1D_2$ and $^3F_3$ bag states, and therefore the f poles, are at $E_L \approx 1000$ MeV, where the Paris potential is inadequate for the long-range interaction and where three-body inelasticity makes coupled-channel calculations of the externally determined f poles technically difficult. Nevertheless the trend of the energy dependence of the wave-function zero in the coupled-channel model is correct.[7]

In the present model the f matrix is calculated for $r \approx \frac{1}{2}\mu^{-1}$ and is taken to have constant components. As stated above this reproduces the poles of the f matrix calculated at $r \approx \mu^{-1}$, the confinement radius, for the $^1S_0$ and $^3S_1$-$^3D_1$ states; and the zeros of the $^1D_2$ and $^3F_3$ wave functions are moving into the confinement radius as those bag-state energies are approached. States confined to the smaller boundary condition radius will have higher energies, and the associated f-matrix poles occur outside the range of energies discussed in this paper. This justifies the energy independence of the shorter-range f matrix.

The agreement of the f-matrix poles calculated in the present model at $r = 1.4$ fm with those of the quark bag model implies that the two models are at least approximately dual for $\frac{1}{2}\mu^{-1} < r < \mu^{-1}$. This is not *a priori* unlikely as condensation into mesons must begin before the radius of complete confinement. This in turn makes the application of asymptotic freedom out as far as the confinement radius suspect. The extension of the Jaffe-Low[36] and Feshbach-Lomon[37] boundary condition approaches to take into account short-range quark degrees of freedom and long-range meson exchange interactions has been discussed.[7] Work on this aspect is continuing and a publication is planned in the near future.

ACKNOWLEDGMENTS

During most of the time of the preparation of the present paper the author was on sabbatical and is most grateful for the hospitality, discussions, and computer and other facilities extended to him by the LAMPF laboratory at Los Alamos Scientific Laboratory, by l'Institut de Physique des Particules Elémentaires of the University of Paris VI, by l'Institut de Physique Nucleáire, Orsay, and by the Department of Physics and Astronomy, University College, London. Conversations with R. Vinh Mau and L. Castillejo helped form the ideas of relationships to the quark bag states. Calculations by M. Lacombe and B. Loiseau provide the information on zeros of the Paris-potential wave functions. This work was supported in part through funds provided by the U. S. Department of Energy under Contract No. DE-AC02-76ER03069.

APPENDIX A: COUPLED-CHANNEL EFFECT ABOVE INELASTIC THRESHOLD

The energy dependence of the attractive contribution of a coupled-channel contribution to the amplitude may be formally obtained by taking the derivative of Eq. (1),

$$\frac{d}{ds}[\Delta\,\mathrm{Re}A_{\alpha L}(s)]=\frac{1}{\pi}\int_{s_i}^{\infty}\frac{\rho_{\alpha L,\alpha' L'}(s')}{(s'-s)^2}ds' \; . \tag{A1}$$

This is formally positive which would indicate an increasing attraction for any s below or above inelastic threshold. But this inference cannot be made if the integral on the right-hand side of Eq. (A1) is divergent.

We assume that the integral converges as $s'\to\infty$. The second-order pole in the denominator assures divergence for $s>s_i$ except for possible zeros of $\rho(s')$. For $s\le s_i$ it is the possible divergence at $s'=s_i$ which must be examined. We therefore consider the integral from s_i to some value s_0 at which the first term in the threshold expansion of $\rho(s')$ still dominates,

$$I_L(s)=\lambda\int_{s_i}^{s_0}\frac{(s'-s_i)^{(L'+1/2)}}{(s'-s)^2}ds' \; , \tag{A2}$$

where λ is a positive constant. The remainder of the integral in Eq. (A1) is weakly dependent on s. Equation (A2) converges for $s<s_i$ and also at $s=s_i$ when $L'\ge 1$, but diverges for $L'=0$ at $s=s_i$. Therefore for all $L'>0$ the increase of attraction with energy persists at threshold, as well as below threshold. As the slope is positive definite at threshold, the increase must continue beyond threshold, as the derivative in continuous for $L'>0$.

The situation for $L'=0$ is more complicated for $s\approx s_i$ as we see by explicit integration of Eq. (1) up to s_0.

$$\Delta\,\mathrm{Re}A_{\alpha 0}(s)=\lambda\int_{s_i}^{s_0}\frac{(s'-s_0)^{1/2}}{s'-s}ds'+\Delta'(s) \; , \tag{A3}$$

where $\Delta'(s)$ is weakly dependent on s. This yields

$$\begin{aligned}\Delta\,\mathrm{Re}A_{\alpha 0}(s)-\Delta'(s)&=2\lambda(s_0-s_i)^{1/2}-\lambda(s_i-s)^{1/2}\tan^{-1}\left[\frac{s_0-s_i}{s_i-s}\right]^{1/2} , \quad s<s_i\\ &=2\lambda(s_0-s_i)^{1/2}-\lambda(s-s_i)^{1/2}\ln\left[\frac{(s_0-s_i)^{1/2}+(s-s_i)^{1/2}}{(s_0-s_i)^{1/2}-(s-s_i)^{1/2}}\right] , \quad s>s_i\end{aligned} \tag{A4}$$

from which it is apparent that the amplitude is increasing for $s<s_i$ and decreasing for $s>s_i$ (see Fig. 6). Equation (A4) also demonstrates the discontinuity in the first derivative at $s=s_i$. For $L'=0$ the attraction due to coupling begins to decrease immediately above threshold.

[1] W. N. Cottingham *et al.*, Phys. Rev. D 8, 800 (1973).

[2] M. Lacombe *et al.*, Phys. Rev. C 21, 861 (1980).

[3] I. P. Auer *et al.*, Phys. Rev. Lett. 41, 1436 (1978); 41, 354 (1978); K. Hidaka and A. Yokosawa, Surv. High Energy. Phys. 1, 141 (1980); I. P. Auer *et al.*, Phys. Rev. Lett. 46, 1177 (1981).

[4] H. Ikeda *et al.*, Phys. Rev. Lett. 42, 1321 (1979).

[5] R. L. Jaffe, Phys. Rev. Lett. 38, 195 (1977); 38, 617(E) (1977).

[6] A. Th. M. Aerts, P. J. G. Mulders, and J. J. de Swart, Phys. Rev. D 17, 260 (1978); 21, 2653 (1980).

[7] E. L. Lomon, in *Comptes Rendus des Neuvièmes Journées d'Études de la Division Physique Théorique, Aussois, 1980,* edited by H. Sazdjian and M. Veneroni (Institut de Physique Nucléaire, Orsay, 1981).

[8] E. L. Lomon, Phys. Rev. D 1, 549 (1970).

[9] E. L. Lomon and H. Feshbach, Ann. Phys. (N.Y.) 48, 94 (1968).

[10] A. M. Green, J. A. Niskanen, and M. E. Sainio, J. Phys. G 4, 1055 (1978).

[11] R. H. Dalitz and S. F. Tuan, Ann. Phys. (N.Y.) 10, 307 (1960).

[12] E. L. Lomon and C. L. Yen, Bull. Am. Phys. Soc. 8, 21 (1963).

[13] J. Wainer and E. L. Lomon, Phys. Rev. D 22, 1217 (1980).

[14] A. E. Wade, S.B. thesis, MIT, 1973 (unpublished).

[15] H. Goldberg and E. L. Lomon, Phys. Rev. 131, 1290 (1963); 134B, 659 (1964).

[16] A. I. Miller and E. L. Lomon, Phys. Rev. D 2, 1245 (1970).

[17] S. Hirschi, Ph.D. thesis, MIT, 1970 (unpublished).

[18] M. Krammer and E. Lomon, Phys. Rev. Lett. 20, 71 (1968).

[19] F. E. Peseckis, S.B. thesis, MIT, 1975 (unpublished).

[20] W. M. Kloet and R. R. Silbar, Nucl. Phys. A338, 281 (1980); A338, 317 (1980) and Phys. Rev. Lett. 45, 970 (1980). These authors include three-particle cut contributions to pion- and heavy-meson-exchange coupled-channel interactions in the $^1D_2$ and $^3F_3$ channels.

[21] (a) W. M. Kloet and J. A. Tjon, Phys. Lett. B106, 24 (1981); B. J. Ver West, Phys. Rev. C 25, 482 (1982). These authors examine the coupling of the $^1D_2$ and $^3F_3$ channels to the $N\Delta$ system via separable potentials. (b) B. J. Edwards and A. N. Kamal, Can. J. Phys. 57, 659 (1979); Ian Duck, Phys. Lett. 106B, 267 (1981). These authors examine the coupling of the $^1D_2$ channel to the $N\Delta$ system via N/D equations.

[22] K. A. Breuckner and K. M. Watson, Phys. Rev. 92, 1023 (1953).

[23] M. Taketani, S. Machida, and S. Ohnuma, Prog. Theor. Phys. (Kyoto) 6, 636 (1951).

[24] M. H. Partovi and E. L. Lomon, Phys. Rev. D 2, 1999 (1970).

[25] M. Brack, D. O. Riska, and W. Weise, Nucl. Phys. A287, 425 (1977).

[26] H. Sugawara and F. von Hippel, Phys. Rev. 172, 1764 (1968); 185, 2046(E) (1969).

[27] R. E. Cutkosky *et al.*, in *Baryon 1980,* proceedings of the 4th International Conference on Baryon Resonances, Toronto, edited by N. Isgur (University of Toronto, Toronto, 1980), p. 19. Similar results were obtained by R. E. Cutkosky *et al.*, Phys. Rev. D 20, 2839 (1979).

[28] S. Hirschi, E. Lomon, and N. Spencer, Comput. Phys. Commun. 9, 11 (1975).

[29] D. V. Bugg *et al.*, Phys. Rev. C 21, 1004 (1980); D. V. Bugg, private communication; R. Dubois *et al.*, Nucl. Phys. A377, 554 (1982).

[30] N. Hoshizaki, Prog. Theor. Phys. 60, 1796 (1978); 61, 129 (1979); K. Hashimoto, Y. Higuchi, and N. Hoshizaki, *ibid.* 64, 1678 (1980); 64, 1693 (1980).

[31] R. A. Arndt and B. J. Ver West, solutions SM80 and SP81 available by commuter access to Scattering Analysis Interactive Dial-in (SAID) at Virginia Polytechnic Institute and State University.

[32] J. Bystricky, F. Lehar, and P. Winternitz, J. Phys. (Paris) 39, 2 (1978); J. Bystricky, C. Lechanoine, and F. Lehar, Report No. DPh P-E 79-01 (unpublished).

[33] M. W. McNaughton *et al.*, in *Polarization Phenomena in Nuclear Physics—1980,* proceedings of the Fifth International Symposium, Santa Fe, 1980, edited by G. G. Ohlsen *et al.* (AIP, New York, 1981).

[34] M. H. MacGregor, Phys. Rev. D 20, 1616 (1979).

[35] D. H. Fitzgerald *et al.*, *Nucleon-Nucleon Interactions—1977,* proceedings of the Second International Conference, Vancouver, edited by H. Fearing, D. Measday, and A. Strathdee (AIP, New York, 1978), p. 91. The result $\delta(^1P_1) = -6.8° \pm 1.1°$ is less repulsive than all the model fits. P. Signell (private communication, 1981) obtains $-8.76° \pm 1.63°$, closer to the model values.

[36] R. L. Jaffe and F. E. Low, Phys. Rev. D 19, 2105 (1979).

[37] H. Feshbach and E. L. Lomon, Ann. Phys. (N.Y.) 29, 19 (1964).